Dual Electron-phonon Coupling Model for Giant Photoenhancements of Dielectric Constant and Electronic Conductivity in $SrTiO_3$

Yu Qiu

Doctor of Philosophy

Department of Materials Structure Science, School of High Energy Accelerator Science, Graduate University for Advanced Studies, 1-1 Oho, Tsukuba, Ibaraki, 305-0801, Japan

September, 2006 (School Year)

Contents

---

* This thesis has been been submitted by Y. Qiu as his doctoral dissertation to the Department of Materials Structure Science, the Graduate University for Advanced Studies.

This doctoral thesis is quoted from the following papers:

1. Y. Qiu, K. Nasu and C. Q. Wu, "Anharmonic soft mode in photoexcited $SrTiO_3$ at low temperatures", Submitted to Phys. Rev. Lett.
2. Y. Qiu, K. Nasu and C. Q. Wu, "Relaxation of ferroelectric domains in photoexcited $SrTiO_3$", Submitted to J. Phys.: Condensed Matter.
3. Y. Qiu, C. Q. Wu and K. Nasu, "Dual electron-phonon coupling model for gigantic photoenhancement of the dielectric constant and electronic onductivity in $SrTiO_3$", Phys. Rev. B **72**, 224105 (2005).
4. Qiu Yu and Keiichiro Nasu, "Theory of super - para - electric large polaron for gigantic photoenhancements of dielectric constant and electronic conductivity in $SrTiO_3$", J. Phys. : Conference Series, **21**, 1 (2005).
5. Y. Qiu and K. Nasu, "Photogeneration of charged ferroelectric domains in quantum dielectric $SrTiO_3$", J. Lumin. **112**, 271 (2005).
6. C. Q. Wu, Y. Qiu, Z. An and K.Nasu, "Dynamical study on polaron formation in a metal/polymer/metal structure" , Phys. Rev. B **68**, 125416 (2003).

Chapter 1

Introduction

Since some 3D type perovkite compounds have been found experimentally to give gigantic dielectric constant, in contrast to ordinary dielectrics, its underlying microscopic mechanism has attractted much attention in the field of solid state theory. As is well-known, the ferroelectric modes play an important roll in the dielectric property, electron transport and phase transition of these materials. Many efforts[1-9] were performed on the connection of this ferroelectric mode with the quartic or sextic anharmonicity. By experiments, gigantic photo-enhancements of the electronic conductivity and the dielectric constant have recently been observed in $SrTiO_3$.[10-12] It was also pointed out that, this dielectric enhancement remains only under the ultraviolet (UV) illumination, while vanishes as the illumination is turned off. As for the photo-induced electronic conduction in $SrTiO_3$, it is expected to be an alternative mechanism from that of the ordinary field induced one in metallic systems. However, the microscopic origin of these photo-induced phenomena has not been clarified theoretically yet. Thus, this is the trigger of the present study.

We will give a short introduction to the soft mode theory in the second chapter, since our work will be based on this theory. The spatial structure and the electronic property of this 3D perovskite, $SrTiO_3$, are also stated, since we will focus our efforts only on this compound in the present work. Some key points of the previous studies on the fundamental properties of $SrTiO_3$, are summerized as well. In Chapter 3, a detailed illustration is given to the Super-Para-Electric(SPE) large polarons, from the set-up of the theoretical model to the

various numerical calculations, and ends up with the impurity effect for this polaron. Then it is followed by Chapter 4, the applications of this SPE polaron theory in the interpretation of the photo-induced giant dielectric constant and electronic conductivity. In Chapter 5, we will discuss the relaxation process of the lattice after the photo-excitation. We will show the formation of the SPE large polaron is an ultra-fast process of about several picoseconds. The evolution of the lattice relaxation is also illustrated numerically. The conclusion is given at Chapter 6.

Chapter 2

Soft Mode Theory

The general condition for the lattice stability of the crystal is that, all normal mode vibrations of this lattice have real and positive frequencies. The limit of stability is approached when the frequency of a mode decreases and approaches zero. Such a mode is referred to as "soft mode". If the frequency of the mode is zero, atoms once displace along that particular mode, there is no restoring force to make them return to their original equilibrium positions. These atoms then reach the new equilibrium positions determined by the symmetry of the mode, and the structure of the crystal changes.

The study of Ferroelectricity has a long history. Except for the excellent phenomenological theory by Mueller[1], Ginzburg[2] and Devonshire[3], the early efforts to describe the ferro-electric transitions were cast in terms of an individual-ion Lorentz-field picture.[13] The stress on a lattice mode depict was first made in the pioneering work of Cochran[14] and Anderson[15] in 1960. They recognized the existence of a soft transverse optic phonon mode of long wavelength and suggested a connection between the strong temperature dependence of this mode near the phase transition and the dielectric anomaly observed in many ferroelectrics. After that, the soft mode theory gained vast applications.[4-9, 16-39]

2.1 Fundamental Knowledge about $SrTiO_3$

Perovskite type solids are a class of important ferroelectrics. They possess a far great dielectric constant, as compared with ordinary dielectrics.[5] This property is usually attributed to the presence of the soft mode in these materials.[14,16,17,21,5,40] Fig. 2.1 gives the structure of the typical 3D perovskite compound, $SrTiO_3$. Since the Ti ion is only loosely boxed up in the octahedral oxygen cage of the perovskite structure, at low temperatures, the restoring force is very small. It is then expected to result in the aforementioned soft mode. With environmental influences, say, an external electric field or a mechanical pressure, the dielectric response of this odd and soft mode will become very large, being the typical characteristic of this material.

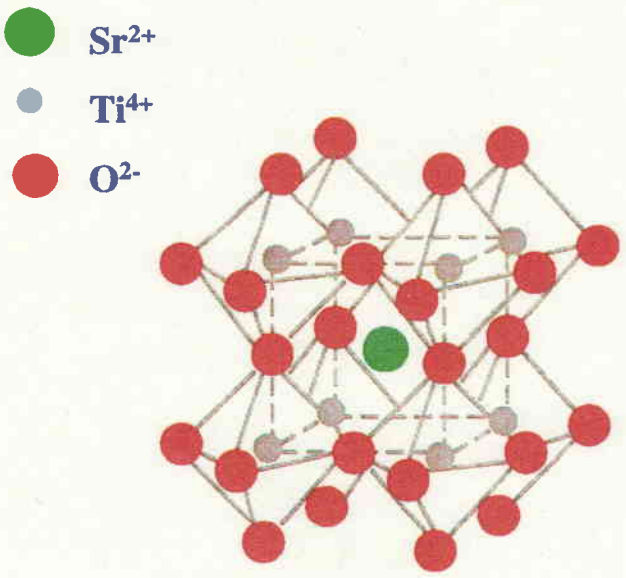

FIG . 2.1. Structure of $SrTiO_3$.

The band structure of $SrTiO_3$ was already calculated by Mattheiss[41] as shown in Fig. 2.2. The top of the valence band of this material is mainly composed of the $2p$ orbital of O, and the bottom of the conduction band is mainly composed of the $3d$ orbital of Ti. In between, there is a wide indirect energy gap of about 3.2 eV. This result was also confirmed by Hasegawa et al.[42].

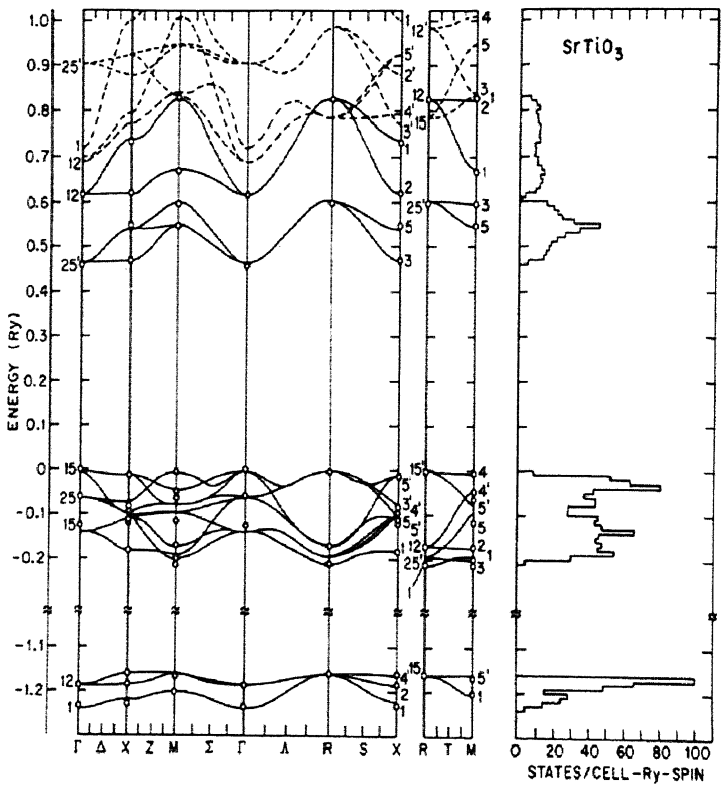

FIG . 2.2. LACO band structure and density of states for $SrTiO_3$.

2.2 Ferroelectric Transition and Quantum Paraelectricity

It is well known that, a ferroelectric transition can usually be associated with the condensation of a soft mode of lattice motion at the Brillouine-zone center. The occurrence of the ferroelectric transition in solids is determined by a competition between cooperative, long-range forces, which try to order the system, and fluctuations, which favor disruption of this order. When the transition occurs at high temperature, i.e., in the classical regime, thermal fluctuation are at work. These fluctuations dominate the high temperature phase and there is

no ordering. However, on lowering the temperature, the fluctuations decrease and eventually the ordering wins, and the system finally orders at a transition temperature, T_c. On the other hand, if the transition occurs at sufficiently low temperature, quantum fluctuations, or zero-point motions, come into play, and they can strongly influence the response of the system.

Since Barrett[43] gave an expression of dielectric constant in perovskite type crystals which seems to be good for all temperatures, there have been considerable theoretical[44-49] and experimental[50-56] efforts devoted to the study of the manifestations of quantum effects on ferroelectric behavior. For general 3D ABO_3 perovskites, on cooling from the high-termperature, high-symmetry phase, the frequency of the soft mode decreases and will ultimately vanish at a transition temperature T_c, thereby transforming the crystal to the low-temperature ferroelectric phase. However for $SrTiO_3$, as is shown in Fig. 2.3 by Müller,[50] it actually does not undergo the ferroelectric phase transition but remain stable against its

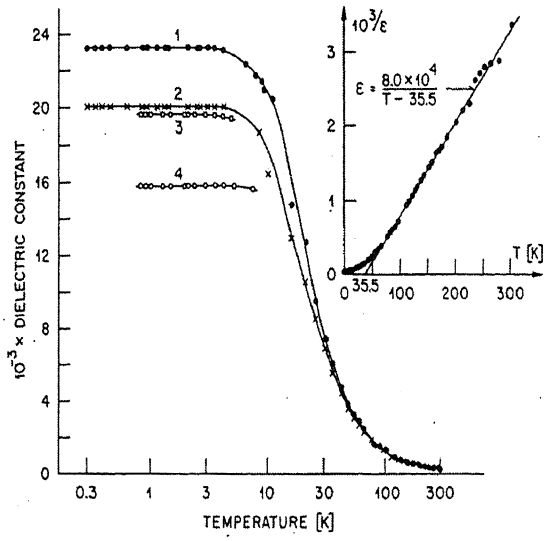

FIG . 2.3. Temperature dependences of dielectric constant ε at 1 bar of $SrTiO_3$.

Inset: $10^3/\varepsilon$ vs T.

ferroelectric soft mode even at ~ 0 K. Hence, $SrTiO_3$ is referred to as an intrinsic quantum paraelectrics. The formation of the quantum paraelectric state is believed to come from the complete suppression of the ordering phase by the quantum fluctuations.[44-46] This is shown in Fig.2.4. As noted, in the high-temperature classical regime the soft mode is stabilized by thermal fluctuations. These fluctuations decrease with decreasing temperature T and ultimately the stabilization vanishes at some T_c, the classical transition temperature designated by T_c^{cl}, as depicted by curve A. However, when T_c dips into the regime of zero-point motion, decreasing T does not appreciably decrease the total fluctuations. Consequently, the high-temperature paraelectric phase will remain below its classical limit, i.e. the transition temperature in the quantum regime, designated by T_c^q, falls below T_c^{cl}. This is depicted by curve B. Ultimately, at low enough temperatures, zero-point fluctuations can suppress the occurrence of the phase transition as shown by curve C.

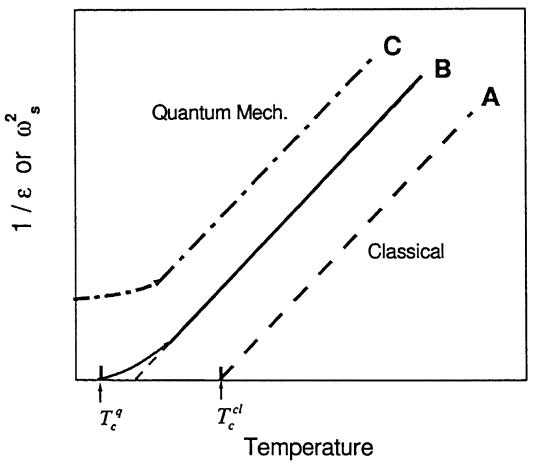

FIG . 2.4. Schematic representation of the suppression of the ferroelectric phase transition temperature by quantum fluctuations.

Since the hypothetical ferroelectric transition temperature of $SrTiO_3$ is very low, the ionic vibrations are expected to have quite a small frequency compared with that of the crystals

with finite transition temperature. The small frequency actually suggests a quite weak restoring force for the soft mode. In order to reflect this weak restoring force, it is expected that the harmonic contribution of the soft mode should be neglected because they will result in a restoring force in proportion to the ionic displacements, which seems too large. So, it is expected that the restoring force should take a nonlinear dependence on the ionic displacements. Thereby, the anharmonic contributions of the soft mode are appropriate for this crystal, say, quartic, sextic or even high order ones.

An ultraviolet light shone to $SrTiO_3$ excites a valence band electron to the conduction band of this material. As mentioned in the above, the top of the valence band are mainly composed of the $2p$ orbits of O^{2-} and the bottom of the conduction band the $3d$ orbits of Ti^{4+}. In the ground state, the electrons are relatively closely bound within the ions to which they belong. While, when an electron is excited to the conduction band, it becomes quite itinerant, extending over the whole crystal. Thus, various lattice vibrations of distinct parities will inflict different influences on this extended electron. It has already been pointed out by Müller[50], that a simple anharmonic (or harmonic) soft mode picture is inadequate for the quantum paraelectricity of $SrTiO_3$ even in the ground state. Therefore, more than one types of phonon modes are expected to take part, especially, in the electronic excited states.

2.3 Sextic Anharmonic Effect in $SrTiO_3$

Many efforts have been devoted to the theoretic model for perovkites.[4-9] One of them is by Vogt[9]. He measured the temperature behavior of the zone-center soft mode of $KTaO_3$ and $SrTiO_3$ between 5 and 300 K by hyper-Raman spectroscopy, and took the results as a stimulus to a refined treatment of the dynamical model of the crystal. For $SrTiO_3$, his result indicates that the sextic anharmonic mode instead of the conventional quartic one becomes a simple but better model so as to reproduce the experimentally observed temperature-dependency of the soft-mode frequency. In our work, as will be carried out, we claim an assurance to the

presence of this sextic anharmonicity by combining the soft mode theory and the photo-generated dielectric and conductive phenomena in $SrTiO_3$.

Chapter 3

SPE Large Polaron Theory

3.1 Photo-induced Phase Transition in $SrTiO_3$

Photo-excitation introduces nonequilibrium phases which possess well-defined long range periodic crystalline or electric order as well as the observable relaxation time in some insulating solids, say, TTF(Tetrathiafuluvalene)-CA(p-Chloranil)[57-59], polymers[60-62], and perovskite type compound[59,10-12]. It is quite different from the static external fields such as magnetic fields or mechanical pressures in material design. Photons have definite momentum, phase, helicity and energy. Hence, they create particular excited states, selectively and intensively. In the case of static external field, it changes all the electronic states of the material, both ground and excited states without selection. In contrast to the chemical design or synthesis, the photoinduced phase transition process realizes new states without changing the chemical composition of the material. Thus the research for photoinduced phase transitions are becoming more and more attractive for material science.[57]

Because of its particular character as a typical intrinsic quantum paraelectricity, $SrTiO_3$ attracted a lot of interest. Recently, Katsu et al.[12] presented the resistivity versus wavelength curve for $SrTiO_3$ as shown in Fig. 3.1. As can be seen, in the ultra-violet range, there is a drastic drop for the resistivity. This indicates that there is a metallic like conduction occurs, i.e., with the ultra-violet irradiation, the crystal undergoes a phase transition from the insulator

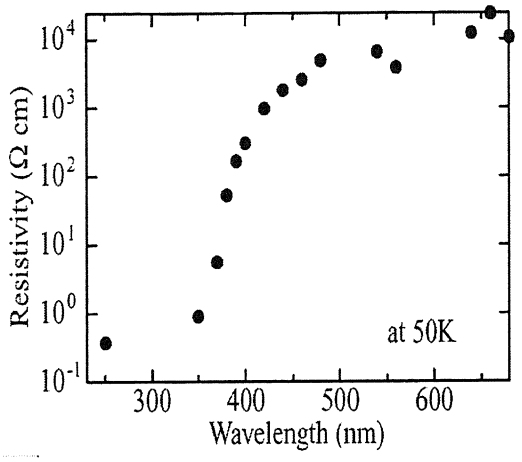

FIG . 3.1. Dependence of photoconduction on wavelengh at 30K.

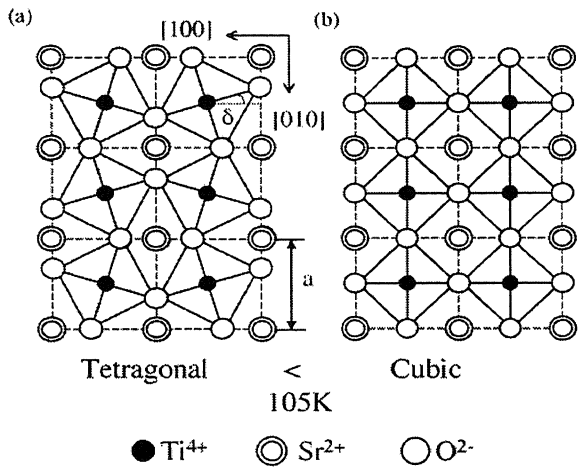

FIG . 3.2. Schematic diagram of the phase transition in STO: (a) tetragonal phase below 105K; (b) cubic phase over 105K.

phase to the quasi-metallic phase.

This phase transition is considered to be concerned with the electronic transport property. Two possible mechanisms were put forward. The first is the increase of photo-carrier generation efficiency caused by the change of the electronic band structure. With the phase transition induced by temperature decrease, it has been proposed that: (1) point R in k-space becomes equal to point Γ[41]; (2) the number of degeneracy of indirect gaps increases; (3) a direct gap becomes an indirect one[63].

The second mechanism is the change of electron mobility accompanied by the phase transition. It is known that $SrTiO_3$ undergoes a second order structural phase transition at 105K[64]. In this cubic-to-tetragonal structural phase transition, neighboring TiO_6 octahedrons are rotated in opposite directions along the c axis by a small angle (δ) as shown in Fig. 3.2. In a cubic system above 105K, the overlap of neighboring 3*d* orbitals is relatively small, but in a tetragonal system below 105K, the overlap is larger because of octahedron rotation, leading to the wider bandwidth. Therefore, this band widening increases the electrical conductivity sharply at the phase transition temperature.

3.2 Luminescence in $SrTiO_3$

A very important experiment is the luminescence in $SrTiO_3$. Hasegawa et al.[42] observed a broad luminescence band at 2.4eV under the band-to-band excitation. No luminescence is observed under the excitation below the indirect gap. This suggests that this luminescence band is intrinsic for this material. Taking account of the broad bandwidth[41-42] and the large Stokes-shift, the origin of the luminescence can be assigned to a recombination of the self-trapped-polaron (STP). This will be elucidated in detail in the following section.

Figure 3.3 gives the temperature dependence of luminescence decay curves in $SrTiO_3$. It is clearly shown that the lifetime of the luminescence can be up to several milliseconds. The decay curves have time dependence expressed in t^{-2} as shown in Fig. 3.3. This suggests that

this decay includes a bimolecular reaction process.[42] The inset of Fig. 3.3 shows time-resolved luminescence spectra observed in 1-2, and in 2 μ s after the photo-excitation. As is shown, there is no difference between the two spectra. This indicates that the origin of the luminescence is always of the same STP state.

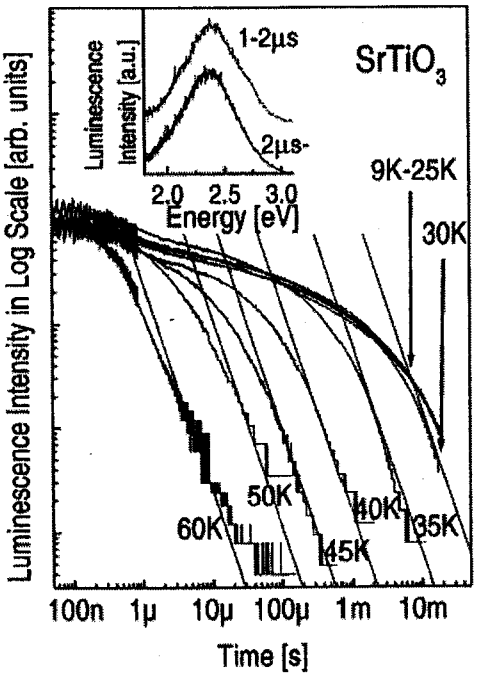

FIG . 3.3. Temperature dependence of luminescence decay curves in $SrTiO_3$. Signals are detected at 500 nm (2.48 eV). Solid lines representing t^{-2} dependence are drawn to guide the eyes. The inset shows time resolved luminescence spectra observed at 4.5 K.

3.3 Photo-induced Dielectric Enhancement

$SrTiO_3$ has already been known to possess far great dielectric constant by comparison with ordinary dielectrics[5]. This is believed to come from its ferroelectric mode[17-20,64]. However,

these phenomena related with the soft mode are concerned only with the electronic ground state of this material. As has been pointed out previously, the way of photo-excitation opens a new window for recognizing interesting stories of materials. It is then expected for the electronic excited states to show some new characteristics. Recently it was found by different groups[10-11] that an ultraviolet irradiation greatly enhances the dielectric constant of $SrTiO_3$. Takesada et al.[10] measured the temperature dependent real dielectric constant as shown in Fig. 3.4 and Hasegawa et al.[42] gave their result in Fig. 3.5. Both of the two experiments

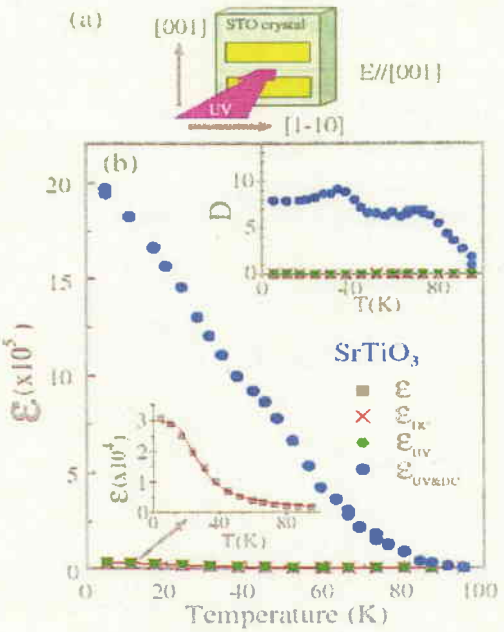

FIG . 3.4. (a) Experimental setup. (b) The temperature dependence of the gigantic real part of the dielectric constant of $SrTiO_3$. ε (black squares), ε_{DC} (red crosses), ε_{UV}(green circles), and $\varepsilon_{UV\&DC}$ (blue solid circles) represent the dielectric constants measured at a frequency f=100 Hz without UV and DC, under only DC, under only UV, and under both DC and UV, respectively. The lower inset shows the temperature dependence of ε in a magnified vertical scale. The solid red curve represents the fit by Barrett's formula.[51] The upper inset shows the temperature dependence of dielectric loss D. The symbols for D also indicate the same experimental conditions as the real part ε .

stated the same fact that with the ultra-violet irradiation, $SrTiO_3$ undergoes a gigantic dielectric enhancement. However, this dielectric enhancement remains only under the ultra-

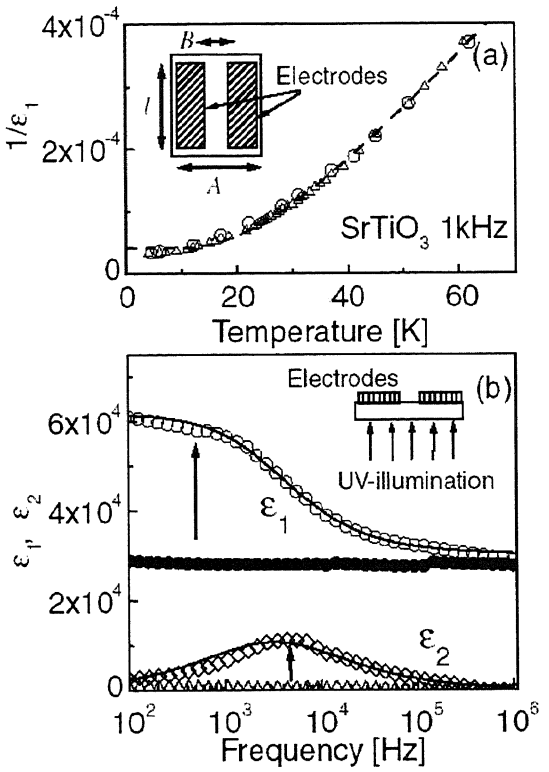

FIG . 3.5. (a) Temperature dependence of the inverse dielectric constant of $SrTiO_3$ measured by parallel electrodes (Δ) and surface electrodes ($\circ$) before UV illumination at 1kHz . The dashed curve is the best fit of Barrett's formula to the data using $T_1 = 72\mathrm{K}$, $T_0 = 32\mathrm{K}$. The schematic picture represents surface electrodes and their dimensions. (b) The dielectric dispersion of $\varepsilon = \varepsilon_1 - i\varepsilon_2$ at 5K, before the UV illumination ε_1 ($\bullet$), ε_2 (Δ) and under the UV illumination ε_1 ($\circ$), ε_2 ($\Diamond$). The solid curves represent the best fit. The schematic picture represents the geometry of electrodes and back-surface illumination.

violet illumination, while vanishes as the illumination is turned off as pointed in the latter work. So, we can also say, this is a kind of photo-induced structural phase transition[57-59] and is expected to come from the coupling between the photo-excited electrons and the aforementioned soft anharmonic phonons of this material[59].

3.4 Dual Electron and Phonon Coupling Model

3.4.1 Band Structure

As we have mentioned that $SrTiO_3$ has a large band gap of about 3.2 eV between the valence and conduction bands. Here we phenomenologically illustrate them by the vacant and shaded rectangles respectively as shown in Fig. 3.6 (b). The experimentally observed long lifetime of the luminescence and the large Stokes-shift (0.8 eV) actually indicate that a couple of electron and hole polaron levels are expected to exist in the large energy gap. We express them with dashed (hole polaron) and solid line (electron polaron) within the energy gap. In the ideal circumstance, the valence band and the conduction band are completely symmetric in the electronic structure. Further, the lattice potential associated with the electron and hole is equal, and comes just from the energy release of the electron and hole respectively during the lattice relaxation process to keep the total energy conserved. Consequently, we can imagine the whole story for the $SrTiO_3$ after photo-excitation as illustrated in Fig. 3.6 (a). With an ultra-violet illumination of the energy of 3.2 eV for a single photon, the valence electron is excited to the conduction band. Then, the valence band is left with a hole and the conduction band becomes negative by a unit charge. Further, due to the lattice relaxation, the electron and hole relax down to the electron and hole polaron states respectively. These relaxations are denoted by the dashed and dotted arrows in Fig. 3.6 (b). Then during a long time, the electron and hole polarons will recombine and gives rise to the luminescence as observed by the experiment[42]. As a result, the system goes back to its adiabatic ground state as designated by

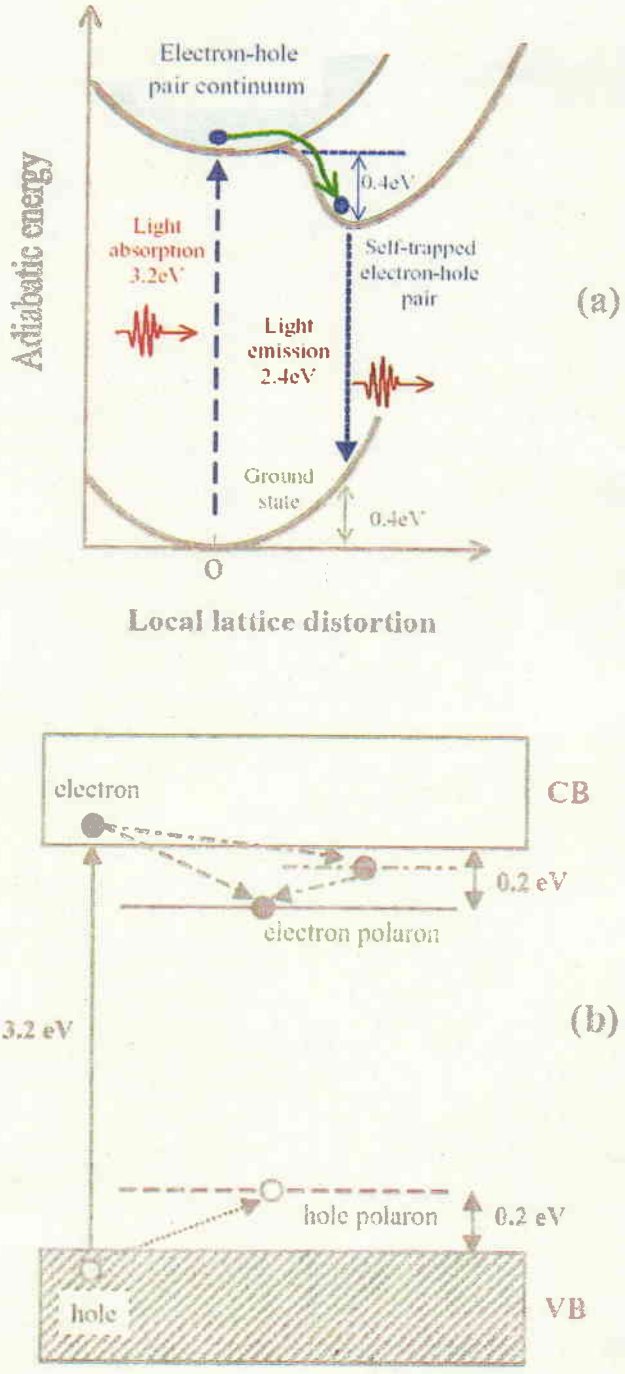

FIG . 3.6. (a)[65] Energy level scheme. (b) Band structure diagram.

the short-dash arrow of Fig. 3.6 (a).

However, we know from Fig. 3.1, that after photo-excitation, $SrTiO_3$ undergoes an abruptly huge enhancement in conductivity. This suggests a free electron-like behavior. However, in this crystal, the electron cannot move in a completely free way because it can never avoid being scattered by phonons. So, it will be more or less trapped by the lattice. Thereby, we could expect a shallow electronic state arise just slightly below the bottom of the conduction band after the photo-excitation, as denoted by the dash-dot line in Fig. 3.6 (b). Thus, we can expect an alternative relaxation route as indicated by the dash-dot arrows in the same figure. It should be noted that there appears another shallow hole state just slightly above the top of the valence band after the photo-excitation, which is not sketched out in the diagram, and the corresponding relaxation route is also absent.

3.4.2 Model Hamiltonian for Conduction Band Electron

A single electron coupling with the phonons in a crystal is usually called a polaron. In ordinary semiconducting and ionic solids, the electron and phonon (*e-p*) interaction exerts great action on their dielectric and transport properties. In connection with the aforementioned optical phenomena in $SrTiO_3$, we think of two typical vibrational modes shown in Fig. 3.7. As shown by Fig. 3.7 (a) the six O^{2-}'s displace along the three rectangular directions in a completely symmetric way, keeping the center of the mass of oxygen ions invariant. This is the A_{1g} mode. Figure 3.7 (b) gives a typical T_{1u} type mode different in parity from the A_{1g} type mode. The six O^{2-}'s of the particular TiO_6 unit will displace along the inverse direction of y axis, while the central Ti^{4+} displaces along y direction. That is, a dipole appears in this TiO_6 unit.

We thus introduce two types of vibration modes into our model Hamiltonian$(\equiv H)$, which describes the electrons in the $3d$ conduction band of $SrTiO_3$, coupling linearly with the aforementioned breathing (A_{1g}) mode and quadrutically with the T_{1u} mode ($\hbar \equiv 1$),

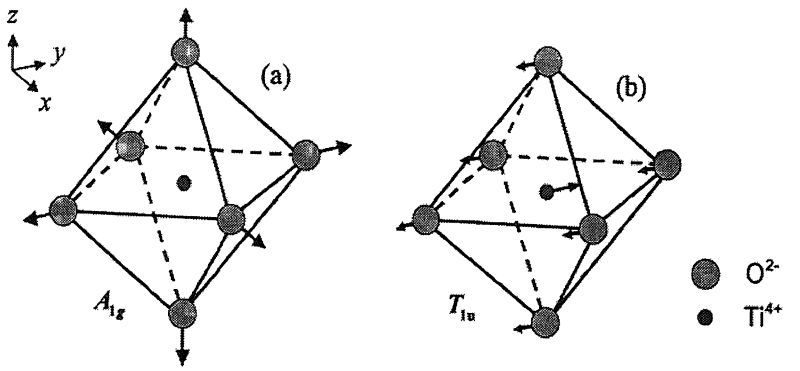

FIG . 3.7. Schematic diagram of the vibration of a single TiO_6 unit for (a) A_{1g} type mode and (b) T_{1u} type mode.

$$H = -T\sum_{\{l,l'\},\sigma}(a_{l\sigma}^{+}a_{l'\sigma}+H.c.)+U\sum_{l}n_{l\alpha}n_{l\beta}-S_b\omega_b\sum_{l}B_l n_l+\frac{\omega_b}{2}\sum_{l}(-\frac{\partial^2}{\partial B_l^2}+B_l^2)$$

$$-\frac{S_d\omega_d}{2}\sum_{l,i}D_{l,i}^2 n_l+\frac{\omega_d}{2}\sum_{l,i}(-\frac{\partial^2}{\beta_m\partial D_{l,i}^2}+\frac{D_{l,i}^6}{3}), \qquad (3.1)$$

$$n_{l\sigma}\equiv a_{l\sigma}^{+}a_{l\sigma},\ n_l\equiv\sum_{\sigma}n_{l\sigma}.$$

Here, $a_{l\sigma}^{+}(a_{l\sigma})$ is the creation (destruction) operator of a conduction band electron at a lattice site l with spin $\sigma(=\alpha,\beta)$ in a simple cubic crystal, and T is the transfer energy between the neighboring two lattice sites l and l' denoted by $\{l, l'\}$. $S_b(>0)$ is the dimensionless constant of the linear coupling between this electron and the site localized breathing mode, whose energy is ω_b and the dimensionless coordinate is B_l. On the other hand, $S_d(>0)$ is the dimensionless constant of the quadratic coupling between the electron and the site localized T_{1u} mode, whose energy is ω_d and the dimensionless coordinate in the direction i (= x, y, z)

is D_{li}. While U denotes the intra-site (intra-3dorbital) Coulomb repulsion. β_m is an effective mass parameter. The dispersions of phonons are neglected, and only the long wave characteristics of each mode are taken into account.

It should be noted that, the T_{1u} mode couples with the $3d$ electron not linearly but only quadratically, due to the symmetry of this mode. While, for A_{1g} mode, there is no such restriction. This quadratic coupling has been already observed by the two-phonon Raman experiment.[66] One can easily infer that, this T_{1u} mode will be related to the dielectric enhancement, while the A_{1g} mode to the luminescence with a large Stokes-shift.

3.4.3 Derivation of the Model

We can always expect a space-inversion symmetry for the Hamiltonian because different choice of the coordinate system does not change the energy of the electron and phonon interacting system. This condition, as will be shown in the following, has an important effect on the normal coordinates of distinct phonon modes. Next, we shall start our model investigation with the A_{1g} type phonon mode as schematically shown in Fig. 3.7 (a).

Within the scheme of the second quantization, the electronic coupling with the Einstein phonons generally reads[67-68]

$$-S\sum_{l} Q_l a_l^{+} a_l \ , \tag{3.2}$$

wherein, S is the general notation of the coupling strength of the *e-p* interaction. Q_l are the normal coordinates of the phonons of the l th quantum state. The normal coordinates Q_l can be expanded by the real displacements of the crystal atoms or ions. For a lattice with N unit cells and s atoms or ions in each, the expansion can be written as

$$Q_{l\eta} \sim \sum_{i=1}^{N}\sum_{\xi=1}^{s} \boldsymbol{u}_{i\xi} \cdot \boldsymbol{h}_{l\eta}^{\xi} e^{-il\cdot R_i^0} \ , \tag{3.3}$$

wherein, $u_{i\xi}$ is the transient vibrating displacement of the ξ th atom or ion in the i th unit cell, whose center of mass coordinate is R_i^0, and $h_{l\eta}^{\xi}$ is the character vector of the corresponding mode.

For $SrTiO_3$, by setting up a rectangular coordinate system with a proper choice of its origin point in the crystal, we can always find an O^{2-} with a transient displacement of $-u_{i_k\xi}$ pertaining to a particular TiO_6 cell centered at $-R_{i_k}^0$, given an O^{2-} with the transient displacement of $u_{i_j\xi}$ pertaining to the cell centered at $R_{i_j}^0$, meeting $u_{i_j\xi} = u_{i_k\xi} = u_{i\xi}$ and $R_{i_j}^0 = R_{i_k}^0 = R_i^0$. From these two O^{2-}'s, we then obtain an I containing only two terms in the summation stated in (3.3)

$$I = u_{i\xi} \cdot h_{l\eta}^{\xi} e^{-il\cdot R_i^0} - u_{i\xi} \cdot h_{l\eta}^{\xi} e^{il\cdot R_i^0} . \tag{3.4}$$

On the other hand, by making a space inversion over the rectangular coordinate system, we can obtain a corresponding two-term summation I' as

$$I' = u_{i'\xi} \cdot h_{l\eta}^{\xi} e^{-il\cdot R_{i'}^0} - u_{i'\xi} \cdot h_{l\eta}^{\xi} e^{il\cdot R_{i'}^0} , \tag{3.5}$$

which meets

$$u_{i'\xi} = -u_{i\xi} ,$$

$$R_{i'}^0 = -R_i^0 . \tag{3.6}$$

Inserting (3.6) into (3.5) yields $I = I'$. Therefore, according to the symmetry of A_{1g} mode, it is clear that $Q_{l\eta}$ keeps invariant by space inversion operation.

Following the same arguments, however, we can prove that for T_{1u} mode, the normal coordinate $Q_{l\eta}$ changes its sign by the space inversion operation. So, we can say, the normal coordinate of T_{1u} mode vibration must enter the Hamiltonian in an even power to keep the energy invariant after the space inversion operation. While for A_{1g} mode, there is no

restriction on the power of its coordinate. As the lowest order approximation, we take linear term for A_{1g} mode and quadratic term for T_{1u} mode and write the *e-p* coupling Hamiltonian temporarily as

$$-S_1\sum_l B_l a_l^+ a_l - S_2\sum_l D_l^2 a_l^+ a_l\ , \tag{3.7}$$

with B_l and D_l representing the normal coordinates of A_{1g} and T_{1u} modes respectively. S_i $(i=1,2)$ are concerned with the electron and phonon coupling strength.

For the time being, we can strategically write the whole Hamiltonian of the *e-p* coupling system in the following way

$$H=-T\sum_{\{l,l'\},\sigma}(a_{l\sigma}^+ a_{l'\sigma}+H.c.)-S_1\sum_l B_l n_l+\frac{S_1'}{2}\sum_l(-\frac{\partial^2}{\partial B_l^2}+B_l^2)$$

$$-S_2\sum_{l,i}D_{l,i}^2 n_l+\frac{S_2'}{2}\sum_{l,i}(-\frac{\partial^2}{\partial D_{l,i}^2}+D_{l,i}^{2r})+U\sum_l n_{l,\alpha}n_{l,\beta}\ . \tag{3.8}$$

Here, we take a harmonic approximation for A_{1g} mode phonons, but for T_{1u} phonons, we, for the present, assume a $2r$th power anharmonicity with r being assumed to be an integer. S_1' and S_2' are the constants related to the effective mass of the two modes respectively.

In order to unravel the boundary condition for the integer *r*, we temporarily make a digression and proceed to the adiabatic property of the system by a variational method.

Under the adiabatic approximation, the Hamiltonian as expressed by (3.8) then reads

$$h_{ad}=-T\sum_{\{l,l'\},\sigma}(a_{l\sigma}^+ a_{l'\sigma}+H.c.)-S_1\sum_l B_l n_l+\frac{S_1'}{2}\sum_l B_l^2$$

$$-S_2\sum_{l,i}D_{l,i}^2 n_l+\frac{S_2'}{2}\sum_{l,i}D_{l,i}^{2r}+U\sum_l n_{l,\alpha}n_{l,\beta}\ , \tag{3.9}$$

For a trial wave function of a polaron state ($\equiv|p\rangle$), we take as

$$|p\rangle=\sum_l \varphi(l)a_{l,\alpha}^+|0\rangle,\quad \sum_l|\varphi(l)|^2=1, \tag{3.10}$$

where $|0\rangle$ is the true electron vacuum, and this $\varphi(l)$ is assumed to be a Gaussian as

$$\varphi(l) \sim \exp[-\frac{\Delta^2(l\cdot l)}{2}], \quad l=(l_x,l_y,l_z), \tag{3.11}$$

wherein, Δ denotes the reciprocal localization length, and l_x,l_y,l_z are the Cartesian components of l. It should be noted here, that $\varphi(l)$ is a localized state when $\Delta>1$ and an extended state when $\Delta<1$. Using this $|p\rangle$, we take the expectation value $\langle h_{ad}\rangle \equiv \langle p|h_{ad}|p\rangle$ and with the Helmann-Feynman theorem

$$\frac{\partial\langle h_{ad}\rangle}{\partial B_l}=0, \quad \frac{\partial\langle h_{ad}\rangle}{\partial D_{l,i}}=0,$$

we can obtain a simple form

$$\langle h_{ad}\rangle=\left\langle -T\sum_{\{l,l'\},\sigma} a^{+}_{l\sigma}a_{l'\sigma}\right\rangle-\frac{S_1^2}{2S_1^{'}}\sum_{l}\langle n_{l\alpha}\rangle^2-\frac{r-1}{r}S_2(\frac{2S_2}{S_2^{'}r})^{\frac{1}{r-1}}\sum_{l,i}\langle n_{l\alpha}\rangle^{\frac{r}{r-1}}. \tag{3.12}$$

In order to give an analytic expression for the adiabatic energy with respect to the extension parameter Δ, we employ the continuum approximation.[59] Within this continuum approximation, l_i $(i=x,y,z)$ can be regarded as a continuous variable from $-\infty$ to $+\infty$. In such a case, (3.12) is reduced to

$$\langle h_{ad}\rangle=\frac{3T\Delta^2}{2}-\frac{S_1^2}{2^{5/2}\pi^{3/2}S_1^{'}}\Delta^3-3S_2(\frac{2S_2}{S_2^{'}r})^{\frac{1}{r-1}}\pi^{\frac{3}{2-2r}}\sqrt{\frac{r-1}{r}}\Delta^{\frac{3}{r-1}}. \tag{3.13}$$

From the preceding two terms of the right-hand side of equation (3.13) it is clear that, at $\Delta>1$, there might exist a minimum on the adiabatic surface. This localized state is just the self-trapped state. However, as we have shown in the phenomenological band structure by Fig. 3.6 (b), for $SrTiO_3$, there is another shallow state appear in the energy gap according to the experimentally measured metallic conduction[12]. In order to theoretically obtain this shallow state, i.e. another minimum on the adiabatic surface in the range $\Delta<1$, it most likely comes

from the combination of the first term and the third term in (3.13), with r being restricted to be greater than $5/2$. Since r is an integer, the choice of the smallest value for r is then 3, i.e., the lowest anharmonicity for T_{1u} phonons is the 6th power. This result is in good agreement with the hyper-Raman scattering experiment.[9] It should be noted that the exclusion of the harmonicity or quartic anharmonicity for T_{1u} phonons is also validated by numerical calculations. The sextic is really the lowest order anharmonicity to produce the shallow extended state in the band gap.

Ultimately, by substituting S_1 and S_2 with $S_b\omega_b$ and $\frac{S_d\omega_d}{2}$, $S_1^{'}$ and $S_2^{'}$ with ω_b and $\omega_d/3$, respectively, we can obtain our discrete model of the Hamiltonian (3.1) from (3.8).

3.4.4 Numerical Confirmation of the Model

In the above section, we have shown the sextic anharmonicity is the best option for the odd parity T_{1u} phonons. However, it seems yet unclear why the lower order cases for this mode are absent in the Hamiltonian. In attempt to get some knowledge about the effect of the lower order terms, we resort to numerically calculating the adiabatic surface of the simplified Hamiltonian

$$H_{sim} = -T\sum_{l,l',\sigma}\{a^{+}_{l,\sigma}a_{l',\sigma} + H.c.\} - \frac{S_d\omega_d}{2}\sum_{l,i} n_l D^2_{l,i} + \frac{\omega_d}{2}\sum_{l,i}(xD^2_{l,i} + \frac{D^6_{l,i}}{3}), \qquad (3.14)$$

wherein, x serves as a ratio to reflect the effect of the harmonic terms on the sextic anharmonic ones.

We employ the Gaussian type trial function for the variance of the degrees of freedom of the soft mode as $D_l = d\exp[-\frac{\Delta_L^2(l\cdot l)}{2}]$. The electronic trial function is already stated in (3.10). For a particular $S_d = 60$, we obtain the corresponding adiabatic surface as shown in Fig. 3.8.

We can see, only when x is very small (~ 0.0001), can the extended electronic state survive. Even if x is as small as 0.001, the extended state will be lifted up into the conduction band. So we can conclude, the introduction of harmonic terms for the soft mode will give rise to too large a restoring force, which will suppress the extended state.

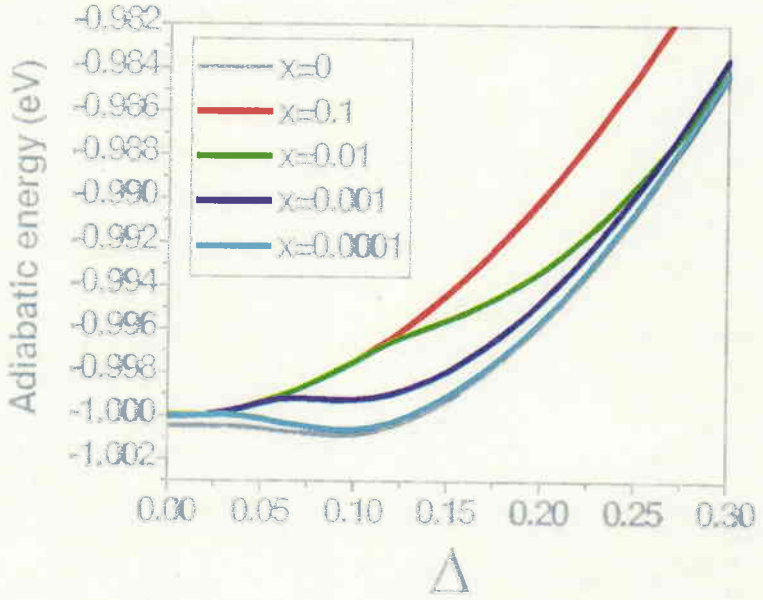

FIG . 3.8 Adiabatic energy of the simplified Hamiltonian for various ratios of the harmonicity to the sextic anharmonicity.

If we replace the harmonic terms $D_{ij}^{2'}$ in (3.14) with the quartic anharmonic terms $D_{ij}^{4}/2$, we can obtain the similar result, except that the critical value for x to suppress the extended state is about 0.01~0.1.

Compared with the sextic anharmonicity, the lower order anharmonic terms or harmonic terms must have a very small ratio if they appear. So we can temporarily neglect them in the investigation of the low temperature properties.

3.5 Unified Theory for Large Polaron and Small Polaron

3.5.1 Adiabatic Surface

Now we rewrite the Hamiltonian of Equ. (3.1) as

$$H = H_{ele} + H_{1g} + H_{1u}, \tag{3.15}$$

$$H_{ele} \equiv -T \sum_{\{l,l'\},\sigma} (a_{l\sigma}^{+} a_{l'\sigma} + H.c.) + U \sum_{l} n_{l\alpha} n_{l\beta},$$

$$H_{1g} \equiv -S_b \omega_b \sum_{l} B_l n_l + \frac{\omega_b}{2} \sum_{l} (-\frac{\partial^2}{\partial B_l^2} + B_l^2),$$

$$H_{1u} \equiv -\frac{S_d \omega_d}{2} \sum_{l,i} D_{l,i}^2 n_l + \frac{\omega_d}{2} \sum_{l,i} (-\frac{\partial^2}{\beta_m \partial D_{l,i}^2} + \frac{D_{l,i}^6}{3}).$$

By this separation, H_{1g} clearly denotes the Hamiltonian for A_{1g} mode and H_{1u} for T_{1u} mode. Since for $SrTiO_3$, its bandwidth (2eV)[41] is far greater than the phonon energy observed in this crystal (~1-10meV)[25,42], we can take the adiabatic approximation. Then from Equ. (3.12), we can obtain the corresponding adiabatic energy of Equ. (3.15) for the single electron system as

$$\langle h_{ad} \rangle = \langle h_{ad} \rangle_{ele} + \langle h_{ad} \rangle_{1g} + \langle h_{ad} \rangle_{1u}, \tag{3.16}$$

$$\langle h_{ad} \rangle_{ele} \equiv -T \sum_{\{l,l'\},\sigma} \langle a_{l\sigma}^{+} a_{l'\sigma} + H.c. \rangle,$$

$$\langle h_{ad} \rangle_{1g} \equiv -\frac{\omega_b S_b^2}{2} \sum_{l} \langle n_{l\alpha} \rangle^2,$$

$$\langle h_{ad} \rangle_{1u} \equiv -\frac{\omega_d S_d^{3/2}}{3} \sum_{l,i} \langle n_{l\alpha} \rangle^{3/2}.$$

The conduction band-width $12T$ is already known to be 2eV from the non-relativistic augmented-plane-wave calculation.[41] According to the absorption spectra,[42] the energy of the breathing mode ω_b is about $20m$eV, and that of the T_{1u} mode ω_d is about $1m$eV from the

Raman scattering.[25] The Coulomb repulsion U is usually one order greater than the charge transfer energy, so we take $U = 4\text{eV}$. β_m is assigned to be 1.294, so that the lowest transition energy between the ground state and the first excited one of the original sextic anharmonic oscillator meets the experimental observation.[25] S_b and S_d are the coupling constants between the electron and these two types of phonons respectively. They, as a set, are to be determined so as to reproduce the observed large Stokes-shift (0.8eV) of the luminescence,[42] i.e. the lowest level of the adiabatic surface has a 0.2eV offset below the bottom of the conduction band. The quadratic coupling, being always subsidiary to the linear one, is assumed to be of the order of 10% of this offset.

3.5.2 Large Polaron and Small Polaron

By absorbing a photon with an energy greater than the band gap of this crystal, a valence band electron is excited to the conduction band. In $SrTiO_3$, such a band like state of electron will immediately decay into other state, because this electron interacts with the phonons, and causes lattice distortions around it.

In the previous work,[59] a continuum model is employed to investigate the adiabatic surface of the single electron system, hence, the degree of localizations of various polaron states are remained unclarified. As a result, the large polaron and the small polaron can never be obtained on the same adiabatic surface. In this connection, we turn to apply a discrete lattice model in the present study.

In practice, we take 1000 lattice sites each along x, y and z directions. First we simply take account the traditionally linear *e-p* coupling model

$$H' = H_{ele} + H_{1g}, \tag{3.17}$$

whose adiabatic energy for the single electron system is

$$\langle h_{ad} \rangle' = \langle h_{ad} \rangle_{ele} + \langle h_{ad} \rangle_{1g}. \tag{3.18}$$

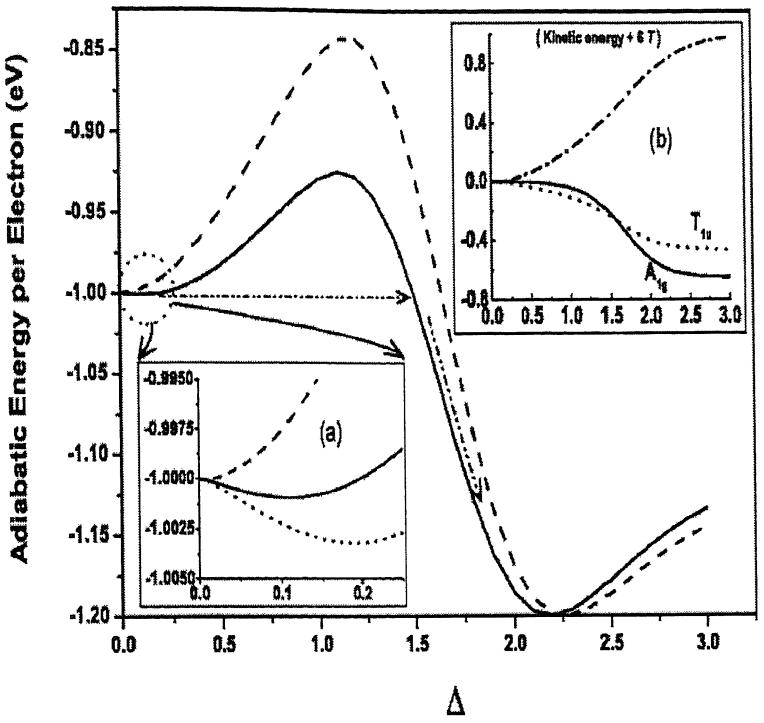

FIG . 3.9. Adiabatic energy per electron with respect to Δ . The solid curve denotes the energy from the dual e-p coupling model. The dashed curve denotes the energy within the linear e-p coupling theory. Inset (a) gives the detailed information of the energy minima in the two curves. A comparison between the single large polaron (solid line or dashed line) and the large bipolaron (dotted line) is also given; (b) shows the contribution of each part of the Hamiltonian of the dual e-p coupling model, solid, dot and dash-dot denote the potential of A_{1g} phonons and their couplings with the electron, the potential of T_{1u} phonons and their couplings with the electron, and the (kinetic energy $+ 6T$), respectively. Parameters are:, $S_b = 9.5$, $S_d = 35.5$.

We can numerically calculate this adiabatic energy for a couple of typical values of S_b and S_d, in accordance with experimental Stokes-shift.[42] In Fig. 3.9, the dashed curve gives the adiabatic surface of the traditional *e-p* coupling model. We can see there are two minima on this curve. As is well known, they just represent the two kinds of polaron states, that is, a large (or free) polaron ($\Delta = 0$) and a small (or here self-trapped) one ($\Delta > 2.0$).

Although the two polaron states are now obtained in a unified way, this large polaron is almost same as the abovementioned band-like plane-wave state. Such a state is actually quite

unstable. By taking into consideration the additional quadratic electron and phonon coupling, this free polaron state will be easily transformed to a more or less slightly trapped state. This is just the so-called super-para-electric (SPE) large polaron state as we will explicate in detail in the immediate section.

3.5.3 SPE Large Polaron and Self-Trapped Polaron

In this section, we proceed to the dual *e-p* coupling model as stated in Equ. (3.15). The corresponding adiabatic energy for the single electron system is shown with the solid curve in Fig. 3.9. At $\Delta = 2.2$, there is the globle minimum, at which the electron is tightly bound almost within one lattice site. This is the off-center type self-trapped polaron, which actually has no difference from the above-mentioned small polaron. However, in the region $\Delta < 1.0$, as we can see clearly from the solid curve in Fig. 3.9 (a), there is a rather shallow bound state, extended over about 1000 lattice sites. This state actually indicates a charged quasi-macroscopic ferroelectric domain. Such kind of charged domain is favorable for polarization. It is called super-para-electric large polaron, abbreviated as SPE large polaron hereafter. The polarized property of the SPE large polaron will be shown in detail in the application part of this dissertation.

In Fig. 3.9 (b), each part of the energy of the one-electron system is given. The solid, dot and dash-dot curves denote the energy from the A_{1g} part, that from the T_{1u} part, and the (electronic kinetic energy + $6T$), respectively. In the region $\Delta < 1.0$, the T_{1u} part is the most dominant. In fact, at $\Delta = 1.0$, the energy from the A_{1g} part is almost zero, which indicates that the large polaron state is determined by a parity violation induced by the quadratic coupling between the photoexcited electron and the T_{1u} phonons. While at the region $\Delta > 1.5$, the effect of the A_{1g} mode rapidly increases, and at $\Delta = 2.2$, it becomes prevailing. That is, the self-trapped state is dominated by the breathing mode.

Besides, the dash-two-dots arrows in Fig. 3.9 represent a quantum tunneling[69] by which the SPE large polaron state can transform into the self-trapped state. This process is shown

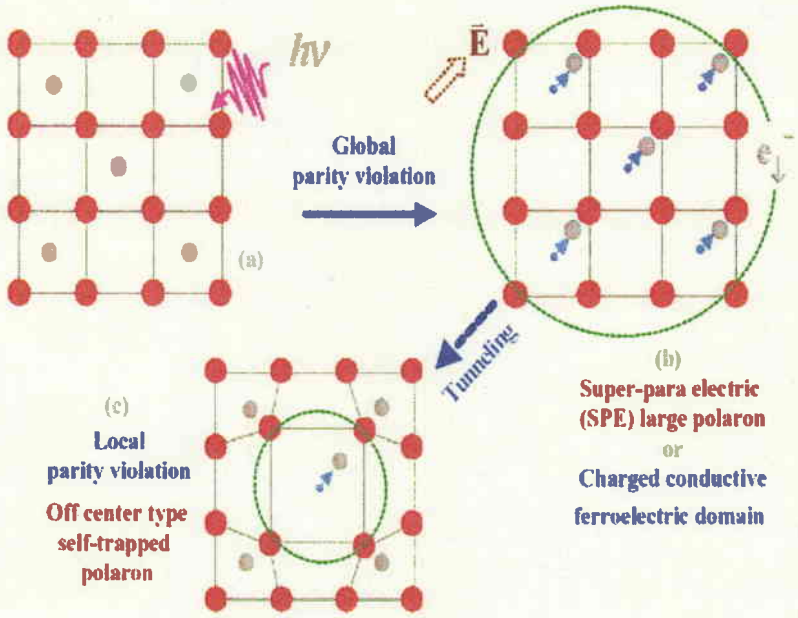

FIG . 3.10. Schematic diagram for local versus global parity violation.[67]

clearly in Fig. 3.10. With the ultra-violet illumination, the crystal, (a), undergoes a globle parity violation and first relaxes down to the SPE large palaron state, (b). As we have shown, this state is actually a charged macroscopic domain dominated by the odd-parity T_{1u} mode. Therefore, it is quite dipole active, say, under an external electric field $\bar{E}$. It is just in this sense that we call it super-para-electric large polaron. In this diagram, the dashed arrow represents the quantum tunneling process, through which the shallow extended state transforms into the self-trapped polaron state, (c). The latter only has a local parity violation as sketched by the small dashed circle.

3.6 SPE Large Bipolaron and Bipolaron Clusters

In contrast to the single electron system, the two-electron system cannot form any strongly localized states, because of the relatively large Coulomb interaction, U. However, two electrons can be loosely bound in an extended state. In order to investigate the many-electron effect, we will next proceed to the two or few electrons cases.

We can write the trial wave function ($\equiv |\Phi_j\rangle$) for a $2j$-electron system ($j = 1,2,4,\cdots$) as

$$|\Phi_j\rangle = \sum_{l_{1\uparrow}\cdots l_{j\downarrow}} \phi_1(l_{1\uparrow})\phi_1(l_{1\downarrow})\cdots\phi_j(l_{j\uparrow})\phi_j(l_{j\downarrow})a^+_{l_{1\uparrow}}a^+_{l_{1\downarrow}}\cdots a^+_{l_{j\uparrow}}a^+_{l_{j\downarrow}}|0\rangle, \tag{3.19}$$

$$\sum_l \phi_j(l)\phi_i(l) = \delta_{ij}.$$

The adiabatic energy per electron ($\equiv h_{adj}$) of this $2j$-electron system is then given as

$$h_{adj} = \frac{1}{2j}\langle\Phi_j|h_{ad}|\Phi_j\rangle = -\frac{T}{2j}\sum_{\{l,l'\},\sigma}\langle\langle a^+_{l\sigma}a_{l'\sigma} + h.c.\rangle\rangle - \frac{\omega_b S_b^2}{4j}\sum_l \langle\langle n_l\rangle\rangle^2$$

$$-\frac{\omega_d S_d^{3/2}}{6j}\sum_{l,i}\langle\langle n_l\rangle\rangle^{3/2} + \frac{U}{2j}\sum_l\langle\langle n_{l\alpha}n_{l\beta}\rangle\rangle, \tag{3.20}$$

where, $\langle\langle\cdots\rangle\rangle \equiv \langle\Phi_j|\cdots|\Phi_j\rangle$. Then, we can obtain the adiabatic surface for the $2j$-electron system by calculating Equ. (3.20), which has been shown by the dotted curve in Fig. 3.9 (a). Since U does not work at all in the extended case, there appear a minimum on this curve as expected. This is just an SPE large bipolaron. It is clearly shown in Fig. 3.11 that the SPE large bipolaron is also a charged macroscopic ferroelectric domain, and dipole active. By the quantum tunneling process, it will fissure into two self-trapped polarons. From Fig. 3.9 (a), we can see that these extended states are very shallow in contrast to the self-trapped one, being metastable states relative to the latter.

In addition, from the energy difference between the two kinds of adiabatic minima in Fig. 3.9 (a), we can expect that two single SPE large polarons will aggregate to form an SPE large bipolaron. Then, it seems natural to ask what happens in the crystal with few bipolarons. For this purpose, we studied a bipolaron molecule composed of two bipolarons with an inter-bipolaron distance($\equiv r$) as shown in Fig. 3.12 (a). The trial functions are assumed as

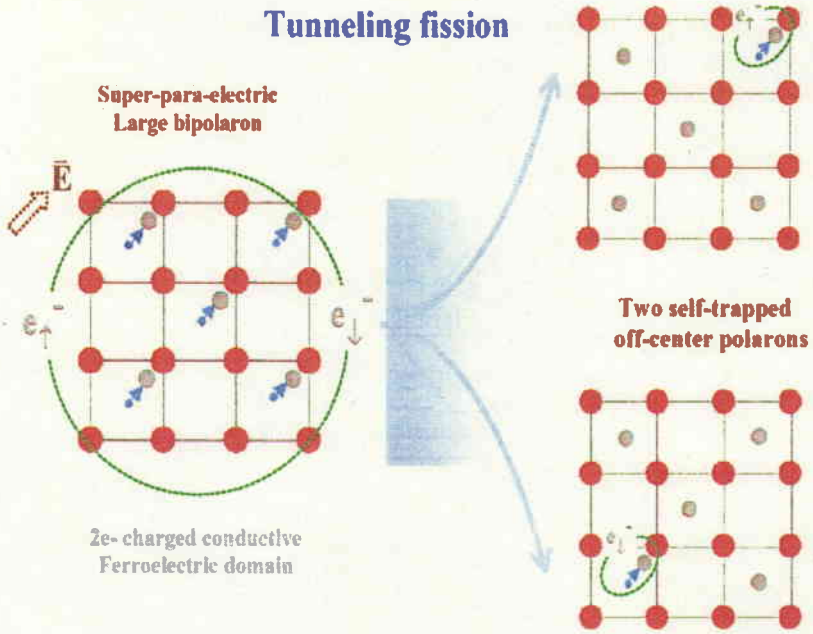

FIG . 3.11. Schematic diagram for SPE large bipolaron fission. [67]

$$\phi_{1\alpha}(l) = \phi_{1\beta}(l) \sim \left\{ \exp\left[-\frac{\Delta_1^2}{2}[l_x^2 + l_y^2 + (l_z + \frac{r}{2})^2] \right] + \exp\left[-\frac{\Delta_1^2}{2}[l_x^2 + l_y^2 + (l_z - \frac{r}{2})^2] \right] \right\},$$

and

$$\phi_{2\alpha}(l) = \phi_{2\beta}(l) \sim \left\{ \exp\left[-\frac{\Delta_2^2}{2}[l_x^2 + l_y^2 + (l_z + \frac{r}{2})^2] \right] - \exp\left[-\frac{\Delta_2^2}{2}[l_x^2 + l_y^2 + (l_z - \frac{r}{2})^2] \right] \right\}.$$

In Fig. 3.13, the solid curve shows the adiabatic energy per electron as a function of r, and it takes minimum at r = 14. Thus, the large bipolaron molecule can be stabilized without changing its large radius.

In order to further elucidate possible SPE large bipolaron clusters, we also investigated a 4-bipolaron molecule with a square structure as shown in Fig. 3.12 (b). The inter-bipolaron distance is also assumed to r. The result is given by the dotted curve in Fig. 3.13. It is almost same as the solid curve. So we can conclude that, before the whole *e-p* system relaxes down to the globally stable self-trapped state, various bipolaron clusters appear. Of course, these

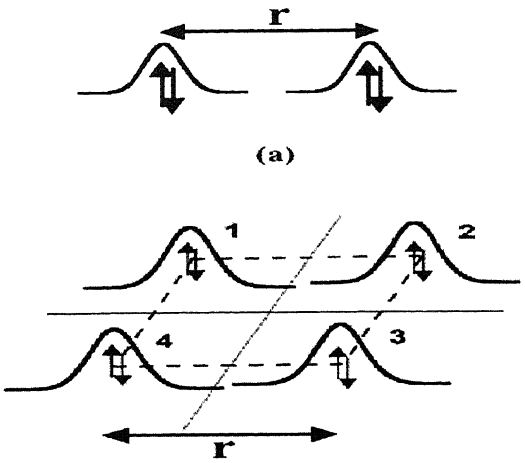

FIG . 3.12. Schematic structure of many-bipolaron system:
(a) Two bipolarons. (b) Four bipolarons.

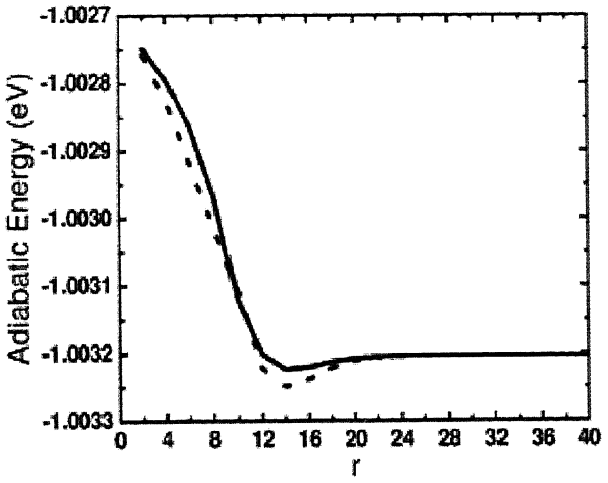

FIG . 3.13. Adiabatic energy per electron of a bipolaron molecule (solid line) and of a square bipolaron molecule (dotted line) with respect to r.

clusters will finally fissure into the off-center type self-trapped polarons through a quantum tunneling[69] process as schematically shown by the dash-dot-dot arrows in Fig. 3.9.

3.7 Impurity Effect

In real experiments, a completely pure material is hard to achieve. Thus, it is important to study the impurity effect in theory. Since some impurity exerts attractive action on electron, it exhibits alike character as the polaron. To distinguish the impurity effect from the intrinsic lowering of the electronic state, we introduce an impurity potential term into the Hamiltonian as following

$$H_{impurity} = -\eta \sum_{\sigma} a_{l\sigma}^{+} a_{l\sigma}, \tag{3.21}$$

wherein, η is the positive potential energy, and l is a particular site at which an impurity is pinned. Here we have the impurity localized at the center of the polaron in order to obtain the globly stable state. Calculations of the adiabatic surface show that the SPE large polaron or bipolaron will not be extincted if the impurity potential is small enough (η<1eV). The consideration of the impurity with small potential only reduces the adiabatic potential barrier between the extended state and the localized one, and causes very small change in the effective radius of the SPE large polaron or bipolaron. This indicates that for $SrTiO_3$, the impurity of small attractive potential does not suppress the SPE large polaron or bipolaron. Our calculation also shows that if η is far greater than 1eV, the globly stable state will get far deep into the energy gap, even lower than the top of the valence band. Such kind of adulterated samples actually make no significance in usual experiments.

Chapter 4

Applications

In this chapter, we will be concerned with the applications of our *e-p* interaction model. In section 4.1, we will first discuss one of the fundamental problems for phonons, phonon softening or phonon hardening with the introduction of *e-p* coupling. In section 4.2, we will apply our SPE large polaron theory to the experimentally observed static dielectric enhancement in $SrTiO_3$, clarifying the microscopic origin of this photo-induced phase transition. In section 4.3, we will give a phenomenological interpretation to the experimentally reported metallic conduction in $SrTiO_3$.

4.1 Phonon Softening and Phonon Hardening

The *e-p* interaction, on the one hand, causes the electron to get into the aforementioned bound state, but, on the other hand, it causes the frequency change of phonons. Next, we will proceed to this phonon frequency change due to *e-p* interaction.

In the SPE large polaron state, Ti ions are correlated with the photo-induced electron, which is itinerant within the macroscopic domain. As a result, this polaron involves a great number of vibration modes. For brevity, first we focus only on a single T_{1u} mode at a typical lattice site, for example, the x direction of the central site of the SPE large polaron, and keep

all coordinates of other modes at their equilibrium positions given by the aforementioned adiabatic theory. So we can get an effective Hamiltonian ($\equiv H'_{1u}$) only for this particular T_{1u} mode

$$H'_{1u} = -S_d \omega_d |\varphi(0)|^2 D^2 + \frac{\omega_d}{2}(-\frac{\partial^2}{\beta_m \partial D^2} + \frac{D^6}{3}), \tag{4.1}$$

wherein, φ is the Gaussian type electronic state announced in Eq. (3.10). In Fig. 4.1, the square-block-curve gives the calculated transition energy ($\equiv E'_{10}$) from the ground state to the first excited state of this single-mode Hamiltonian with respect to S_d. It is shown that the electronic coupling with the anharmonic T_{1u} mode in a quadratic manner does cause softening of this mode. The stronger the quadratic coupling strength is, the greater the softening gets. However for the A_{1g} mode

$$H'_{1g} = -S_b \omega_b |\varphi(0)|^2 B + \frac{\omega_B}{2}(-\frac{\partial^2}{\partial B^2} + B^2), \tag{4.2}$$

our calculations show there is neither softening nor hardening occur. This can be easily understood in that we have shown A_{1g} mode plays the dominant role in the localized state. In such a state, the electron is tightly bound within one lattice site. On the contrary, the lattice is also tightly bound by the trapped electron. As a result, the phonon energy structure is relatively stable.

Our calculation results also show that in the self-trapped polaron state, the anharmonic T_{1u} mode quadratically coupling with the electron will result in degeneracy in low phonon energy levels, which actually leads to phonon hardening. This effect in itself will prevent the dielectric enhancement as schematically shown in Fig. 4.2. However, since this phonon hardening happens in the self-trapped state, essentially it will not affect the dielectric property of the material as will be elucidated in the following section.

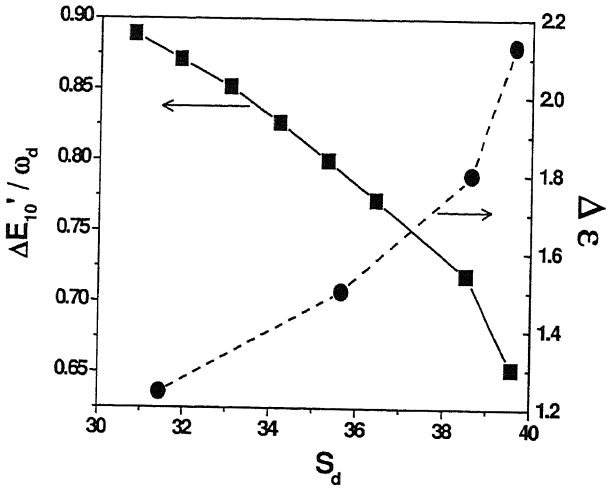

FIG . 4.1. Square blocks are for Phonon softening: $\Delta E'_{10}$ versus S_d. $\Delta E'_{10}$ is the energy difference between the ground state and the first excited state of the single sextic oscillator coupled with the electron quadratically. Filled circles are for dielectric ratio $\Delta\varepsilon$ with respect to S_d.

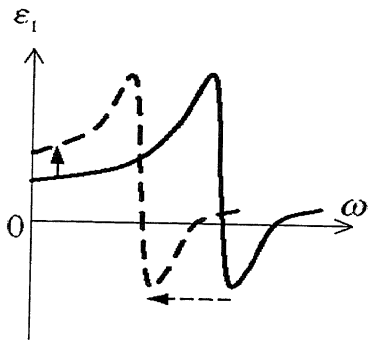

FIG . 4.2. Schematic static dielectric enhancement with respect to phonon softening. Solid and dashed curves denote the frequency dependent dielectric constant before and after the introduction of the e-p coupling respectively. Dashed arrow shows the direction of phonon softening. Solid arrow shows the increasing direction of the static dielectric constant.

4.2 Static Dielectric Enhancement

In order to reflect the variance of dielectric constant, we define a ratio $\Delta\varepsilon$ $(\equiv \varepsilon'_1 / \varepsilon_1)$. Where, ε'_1 represents the static dielectric constant resulted from H'_{1u} and ε_1 the static dielectric constant from the original T_{1u} mode, whose Hamiltonian $(\equiv H_{1u})$ is already given as

$$H_{1u} = \frac{\omega_d}{2}\left(-\frac{\partial^2}{\beta_m \partial D^2} + \frac{D^6}{3}\right). \tag{4.3}$$

ε_1 can be approximately calculated by

$$\varepsilon_1 \sim \sum_m \frac{|D_{m0}|^2}{\Delta E_{m0}}. \tag{4.4}$$

Here, D_{m0} is the matrix element of dipole transition from the vibrational ground state to the mth excited state, and ΔE_{m0} is the energy difference between them.

In Fig. 4.1, the dots depict $\Delta\varepsilon$ versus S_d. As is seen, The static dielectric constant averagely increases by a half, and our calculations indicate that this increase mainly comes from the softening suggested by the blocks in the same figure. This can be seen more clearly in Fig. 4.2. The dashed arrow shows the direction of phonon softening. At the same time, the static dielectric constant is increased as instructed by the solid arrow. However, it should also be noted here, that this enhancement of the static dielectric constant results only from one typical T_{1u} mode, as we have mentioned in previous discussion. Actually, the SPE large polaron is a macroscopic domain with hundreds and thousands of lattice sites involved. We have validated that, at each lattice site, this T_{1u} mode will be softened by the $e-p$ interaction, and as such results in huge dielectric enhancement respectively. Their corporative effect gives rise to a gigantic enhancement in the macroscopic static dielectric constant, which

has been observed experimentally.[42] It should be mentioned that this photo-enhancement of static dielectric constant occurs also in the SPE large bipolaron, or in other large polaron clusters.

As for the off-center type self-trapped polaron, the electron is tightly bound almost within one lattice site. Therefore, only few soft T_{1u} modes are involved. As a result, the extra *e-p* coupling almost brings out no macroscopic dielectric change although there appear a phonon hardening, instead of phonon softening in this case as stated previously. This agrees with the experimental fact that when the ultraviolate illumination is turned off, the phenomenon of dielectric enhancement disappears.[42] The reason is that there will be no new SPE large polarons created after the turn-off of the ultraviolet illumination, and the existent SPE large polarons and bipolarons incline to transform into the self-trapped polarons by a quantum tunneling process.[69]

From the above discussions, we can see that the enhancement of static dielectric constant comes from the phonon softening, and the latter is due to the introduction of $e-p$ coupling. However, phonon softening happens only to the T_{1u} mode in the SPE large polaron state. Therefore, we can say, the enhancement of static dielectric constant comes mainly from the sextic anharmonic oscillator coupled with the photo-induced electron. This functional distinction actually results from the difference of parity. The T_{1u} mode of odd parity is easy to be polarized and thus inclines to give rise to a conspicuous dipole. While, the A_{1g} mode has an even parity, and remains free from the polarization, even under an external electric field.

4.3 Photo-induced Metallic Conduction in $SrTiO_3$

As is known, in the absence of the scattering of phonons, the conduction electron moves freely under an external electric field. However, with the account of the $e-p$ interaction, the conduction band electron will distort its nearby ions and results in lattice displacement

around it. On the contrary, the electron might get heavier because whenever it moves there will be an induced lattice displacement dragged by it. This is just the mass enhancement of the polaron. In order to clarify this mass enhancement effect, we next study a one site translation motion of the polaron by calculating the expectation value of the electronic transfer operator $\sum_l a_{l\sigma}^{+} a_{l+1,\sigma}$ between two polaron states with neighboring centers as schematically shown by the big dashed and big solid circles in Fig. 4.3. We define a ratio between the real polaron transfer and the hypothetical bare electron transfer as

$$R = \frac{\langle \Psi' | \sum_l a_{l\sigma}^{+} a_{l+1,\sigma} | \Psi \rangle}{\langle \Psi'_{ele} | \sum_l a_{l\sigma}^{+} a_{l+1,\sigma} | \Psi_{ele} \rangle}, \tag{4.5}$$

wherein, $|\Psi_{ele}\rangle$ is the electronic state and $|\Psi\rangle$ is the polaron state encompassing both electronic and phonon configurations. The state with a prime distinguishes from that without a prime by the center of the polaron. The Hamiltonian of the e-p coupling system generally involves the charge transform, phonon energy and the e-p interaction part. If we take the e-p interaction as the mean field on the phonons, then under Hartree-Fork approximation, the polaron state can be reduced to the direct product of the electronic state and the phonon state as $|\Psi\rangle = |\Psi_{ele}\rangle \cdot |\Psi_{ph}\rangle$. The ratio R is then reduced to the inner product of the two phonon states, i.e., $R = \langle \Psi'_{ph} | \Psi_{ph} \rangle$. The state $|\Psi_{ph}\rangle$ encompasses many modes of T_{1u} type as well as A_{1g} type modulated by the $e-p$ couplings. Namely,

$$\langle \Psi'_{ph} | \Psi_{ph} \rangle = \left[\prod_l \langle \Psi_{T_{1u}}(l) | \Psi_{T_{1u}}(l+1) \rangle \right]^3 \left[\prod_l \langle \Psi_{A_{1g}}(l) | \Psi_{A_{1g}}(l+1) \rangle \right], \tag{4.6}$$

wherein, $|\Psi_{T_{1u}}(l)\rangle$ are the phonon ground states of the modulated single T_{1u} modes with the effective Hamiltonian

$$H'_{1u}(l) = -S_d \omega_d |\varphi(l)|^2 D^2 + \frac{\omega_d}{2} \left(-\frac{\partial^2}{\beta_m \partial D^2} + \frac{D^6}{3} \right), \tag{4.7}$$

and $\left|\Psi_{A_{1g}}(l)\right\rangle$ are the phonon ground states of the modulated single A_{1g} modes with the effective Hamiltonian

$$H'_{1g}(l) = -S_b\omega_b\left|\varphi(l)\right|^2 B + \frac{\omega_b}{2}\left(-\frac{\partial^2}{\beta_m \partial B} + B^2\right). \tag{4.8}$$

In Fig. 4.4, we give the result of R versus S_d for the self-trapped polaron as well as for the SPE large polaron. For the case of SPE large polaron denoted by square blocks, R has almost no deviation from 1, which indicates a quite similar behavior to that of the free conduction band electron. It suggests that the SPE large polaron has almost no mass enhancement. With the onset of ultraviolet radiations, many charged SPE large polarons will be created. They move smoothly under an external electric field and contribute to the high electronic conductivity. This conductive property of SPE large polaron is also applicable to the SPE large bipolaron, and can be employed to understand the observed large photo-conduction in $SrTiO_3$.[12] For the case of self-trapped polaron as denoted by triangles, R is almost 0. This indicates a gigantic mass enhancement, because the electron is tightly bound within a lattice potential well and entails very strong external electric field to help it break away from the bondage. This also suggests a perspective disappearance of the photo-current in $SrTiO_3$ when the ultraviolet irradiation is removed.

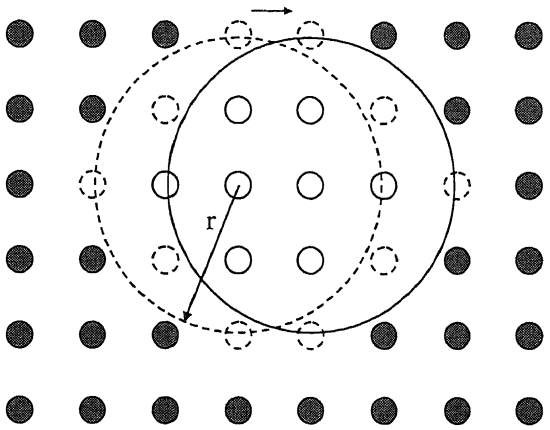

FIG . 4.3. Schematic diagram of polaron shift. Big circles denote the effective range of the polaron. Small filled circles denote bare phonon modes, and small unfilled circles denote the modes coupled with the electron.

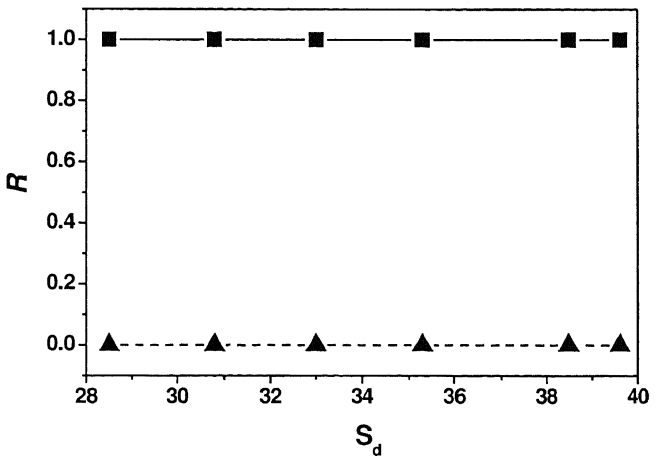

FIG . 4.4. S_d-dependent ratio R, triangles are for self-trapped polaron and square blocks are for SPE large polaron.

Chapter 5

Lattice Relaxation Process

In this chapter, we aim to discuss the relaxation of the crystal lattice after photoexcitation. It has already been studied that for polymers, the formation of the polaron or exciton is an ultra-fast process.[61] In experiment, these states could be detected and predicted from the spectra. However, by virtue of the molecular dynamics theory, the information of the lattice configuration as well as the electronic state can be traced so as to compare with the energetic evolution. Then, the lattice relaxation process could be recognized more clearly. In section 5.1, we will give a description to the molecular dynamics theory for the e-p interacting system. In section 5.2, we will apply this method to $SrTiO_3$ and give some detailed descriptions about the relaxation process in this crystal.

5.1 Molecular Dynamics

Photo-excitation brings forward rich phenomena especially for ionic crystals. The excited electrons induce lattice distortions with the introduction of e-p interactions. This is just the lattice relaxation process. Various relaxation paths arise from different conditions, the initial lattice configurations, the preliminary electronic states and the electron and phonon interactive mechanisms.

Usually, the e-p coupling system will undergo a great number of meta-stable states. Then through the quantum tunneling process, these states will transform into other relatively stable states, say, the globally stable states. The system can remain in such kind of states for relatively long period. After this period, the system will finally come back to its ground state through luminescence or non-irradiative decay process.

On the other hand, under certain conditions, the system does not undergo such complicated relaxation process. The electron can find a direct route without any medium state from the conduction band to the valence band, releasing its energy to the lattice in the form of phonons.

In experiment, various medium states could be observed and/or predicted from various spectra. However, the detailed relaxation process is generally left unclear. Starting from the properly chosen model, molecular dynamics method can reappear the evolutions of the lattice configuration as well as of the electronic state. SSH[70] model has been proved to be a successful model for one dimentional system such as polymers, and the molecular dynamics method has gained important applications in investigating the quasi particles, say, solitons, [71] excitions[72] and polarons,[61] in such kind of materials.

Since the electron has far less inertia relative to the phonon, especially in complex ionic crystals, the relaxation process can be taken as an adiabatic process. Thus, for any particularly given lattice configuration $\{\equiv\Theta_l\}$, of some transient time, the electronic state can be described by the combination of the eigen states out of this lattice potential.

If we take the Hamiltonian as

$$H = H_{electron}(\{\Theta_l(t)\}) + H_{potential}(\{\Theta_l(t)\}) + H_{kinetic}(\{\dot{\Theta}_l(t)\}), \tag{5.1}$$

the total Hamiltonian is composed of three parts, the electronic Hamiltonian $H_{electron}(\{\Theta_l(t)\})$, being the function of the lattice configuration $\{\Theta_l(t)\}$ by encompassing the e-p coupling terms, the lattice potential $H_{potential}(\{\Theta_l(t)\})$ and the lattice kinetic energy $H_{kinetic}(\{\dot{\Theta}_l(t)\})$. As just discussed, the relaxation process can be regarded as an adiabatic process. So the

electron and the phonons can be handled separately. The electronic eigen states $(\equiv \varphi_n(t))$ satisfy the following equation

$$H_{electron}(\{\Theta_l(t)\})\varphi_n(t) = \lambda_n(t)\varphi_n(t). \tag{5.2}$$

If the relaxation starts from the Frank-Condon state, the electron can be regarded always to be at the lowest eigen state.

For the lattice, it evolves in terms of the Newtonian equation

$$M_l\ddot{\Theta}_l(t) = f_l(t), \tag{5.3}$$

$$f_l(t) = -\frac{\partial}{\partial\Theta_l(t)}\langle\Psi(t)|H|\Psi(t)\rangle,$$

with M_l being the effective mass for the lth lattice site and $f_l(t)$ the transient force on it. As a result, the evolution of the e-p coupling system can be obtained by numerically calculating the coupled equations (5.2) and (5.3).

Practically, given small enough time span τ, the lattice evolution can be handled by the general differential method as

$$\dot{\Theta}_l(t+\tau) = \frac{f_l(t)}{M_l}\tau + \dot{\Theta}_l(t),$$

$$\Theta_l(t+\tau) = \dot{\Theta}_l(t+\tau)\tau + \Theta_l(t). \tag{5.4}$$

$SrTiO_3$ is a perovskite type complex. It has been confirmed to possess a large indirect gap over 3eV both theoretically[41] and experimentally[42]. With the introduction of e-p interaction, it is then expected to bring about rich phenomena in such a large energy gap. To understand the microscopic evolution process in the crystal, the above mentioned molecular dynamics method can be applied to the corresponding e-p coupling system. Combining the Hamiltonian (3.1), we can obtain the relaxation picture of this crystal acted by photoexcitation.

5.2 Relaxation of the Electron and Phonon Coupling System

In this effort, we mean to investigate the polaron effect during the relaxation process. So we carry out the dynamics only for the single electron system. In such a case, the photo-excited electron is assumed initially to be in the bottom of the conduction band. Although this electron is in a quasi plane wave state, the real crystal can always approximate to an infinite region for the electron, and the electronic motion concerned region is only a small part of the crystal. This picture is illustrated in Fig. 5.1. The black circles denote the region within which the electron transfers from site to site and couples to the lattice. Lattice vibrations in such a region are described by the dressed phonons. In contrast, the blue circles denote the region in

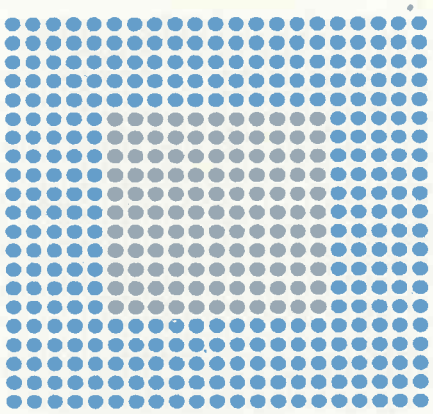

Fig. 5.1. Schematic diagram of the e-p coupling system.

which the lattice has not any interaction with the electron. Lattice vibrations in this region are described by the bare phonons. The blue region actually serves as the thermal reservoir. In contrast, the black region is regarded as the system in the following.

By replacing the kinetic operator $\frac{\partial^2}{\partial B_l^2}(\frac{\partial^2}{\partial D_{l,j}^2})$ with the corresponding classical expression $\dot{B}_l^2(\dot{D}_{l,j}^2)$, the Hamiltonian (3.1) is transformed into the following

$$H \equiv -T\sum_{\{l,l'\}}(a_l^+ a_{l'} + h.c.) - S_b\omega_b\sum_l B_l n_l + \frac{1}{2}\sum_\ell (K_B B_\ell^2 + M_B \dot{B}_\ell^2) - \frac{S_d\omega_d}{2}\sum_{l,i} D_{l,i}^2 n_l$$

$$+\frac{1}{2}\sum_{\ell,i}(K_D D_{\ell,i}^6 + M_D \dot{D}_{\ell,i}^2) + \frac{1}{2}K_{BB}\sum_{\{\ell,\ell'\}} B_\ell B_{\ell'} + \frac{1}{2}K_{DD}\sum_{\{\ell,\ell'\},i,i'} D_{\ell,i}^3 D_{\ell',i'}^3 , \qquad (5.5)$$

where the summation index l runs over the black region and the index ℓ over the whole region containing the black and the blue in Fig.5.1. The expression $\{\cdots,\cdots\}$ indicates the summation is over the nearest neighboring sites. The last two terms in (5.5) are introduced so that the energy can transmit within the whole crystal in the form of phonons. They actually realize the damping during the real dynamics process.

If the Plank constant $\hbar$ is forced to be a dimensionless constant, $\hbar \equiv 0.6591$, then fs^{-1} is equivalent to eV. In consequence, we have the elastic coefficients $K_B \sim \omega_b$ and $K_D \sim \frac{\omega_d}{3}$, and the effective masses $M_B \sim \frac{\hbar^2}{\omega_b}$ and $M_D \sim \frac{\beta_m \hbar^2}{\omega_d}$. Usually, $K_{BB}\,(K_{DD})$ is one order less than $K_B\,(K_D)$, so practically we take $K_{BB} = K_B/10$ and $K_{DD} = K_D/10$.

As previous, the e-p coupling system is assumed to start from the Frank-Condon state with zero phonons, and the electron starts from the bottom of the conduction band. With the size of $5\times5\times5$ for the system and $21\times21\times21$ for the total crystal, we obtain the energy evolution curve of this e-p coupling system as shown in Fig. 5.2. We calculated 10,000 steps with the step of 1 fs. As shown in Fig. 5.2, with time, the total energy is conserved, while the energy of the system decays gradually. However, after 2000 fs, it reaches a stable value of about -1.018eV. This is because the electron induces the lattice vibrations first in the e-p coupling system. Then these vibrations are gradually transmitted to the whole crystal and the energy contained in the lattice is prone to be evenly distributed. This is just the essence of damping in crystals.[73]

This value of -1.018eV actually implies a meta-stable bound state. Figure 5.3 gives the electronic distribution in space at different time. It is clearly shown that the relative difference

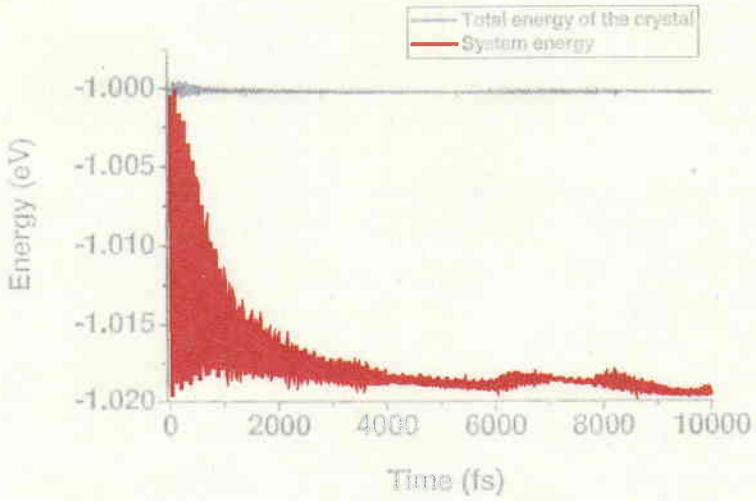

Fig.5.2. Energy evolution diagram. Black line indicates the total energy conservation. Red curve stands for the evolution of the energy within the e-p coupling region (5×5×5). Parameters are : S_b=19.1, S_d=10.5.

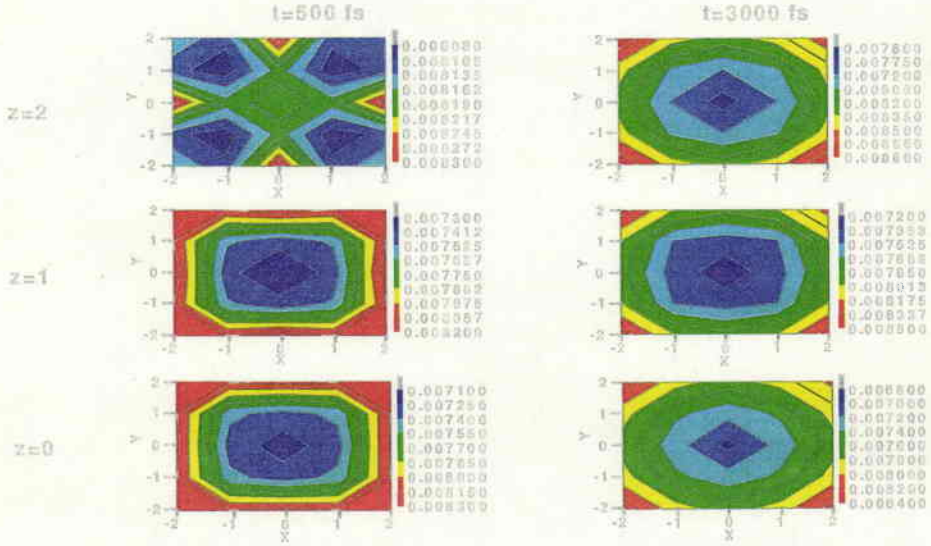

Fig. 5.3. Electronic distribution within the *e-p* coupling region (5×5×5).

of the charge distribution at distinct sites is very small during the relaxation. This suggests the electron consists always in an extended state. It is just the SPE large polaron state.

From the above discussions, we can see the relaxation of the SPE large polaron in the 3-dimensional $SrTiO_3$ crystal is also a ultra-fast process. It is of the pico-second order. This is why with the ultraviolet irradiation, $SrTiO_3$ will immediately exhibit an enhanced dielectric character as well as the extra-ordinary conductive ability, combined with the previous conclusions.[10-12,74]

Chapter 6

Conclusion

Here, it is worth mentioning that the sextic potential for the T_{1u} mode in our model is a necessity. It is the lowest order choice for the anharmonicity because a substitution of quartic anharmonicity for this T_{1u} mode will suppress the extended state in the energy gap. Therefore, the quartic anharmonicity cannot reflect both the conductive and the dielectric property of $SrTiO_3$. Instead, the sixth or higher order anharmonicity is the nature to this crystal. This result is in quite good agreement with the hyper-Raman experiment.[9]

In summary, we employed a discrete lattice model to investigate a dual *e-p* interacting model for $SrTiO_3$. The photo-generated electron is assumed not only linearly coupled with the A_{1g} phonons but also quadratically coupled with the T_{1u} phonons, which results in two kinds of polarons, the SPE large polaron and the off-center type self-trapped polaron. In terms of the energy difference, two SPE large polarons are expected to aggregate to form an SPE large bioplaron. The SPE large bipolaron is shown to be the most stable quasiparticle state for the many electron systems. Many SPE large bipolarons will not constitute even large polaron, instead, they will form various clusters. The SPE large polaron, bipolaron and bipolaron clusters are all dipole active. The photo-excited electrons interact with the phonons and the e-p coupling system reaches the SPE large polaron or bipolaron state first because it is energetically close to the Frank-Condon state. In these extended states, the quadratic *e-p*

coupling results in the softening of the T_{1u} mode. This softening causes gigantic static dielectric enhancement in $SrTiO_3$. However, in the localized state, the dielectric property will not be changed. These results are in agreement with the experimental phenomenon. Calculations of the ratio R show that the SPE large polarons or bipolarons contribute to large photo-conduction, while the self-trapped polarons are immobile. In addition, the impurity with a small attractive potential ($\eta < 1\text{eV}$) does not suppress the SPE large polaron and bipoalron states. The introduction of the impurity only tends to reduce the barrier between the extended state and the localized state and the poalron effect can never be neglected for $SrTiO_3$. Therefore, the impurity does not seriously alter our present conclusions.

The dynamics study of $SrTiO_3$ indicates the formation of the band states is an ultra-fast process of the picosecond order.

Acknowledgements

First I would like to give my sincere thank to Professor Keiichiro Nasu for guiding me into this challenging field. And I must owe my accomplishment in this work to the timely discussions with him and his sagacious guidance. I would also like to thank Professor Changqin Wu for generously sending me his manuscripts with his insights. And I would like to acknowledge Professor N. Tomita, Dr. K. Iwano, Dr. K. Ji, Dr. K. Nishioka, Dr. J. G. Han and Mr. J. F. Yu for helpful discussions and Dr. M. Yamazaki and Dr. R. Yabuki for their kind help in intranet business. Finally, I would like to owe my debts to my family. I could not have spent the three years smoothly overseas without their love and understanding.

References

[1] H. Mueller, Phys. Rev. 57, 829 (1940); 58, 565 (1940); 58, 805 (1940).

[2] V. L. Ginzburg, Zh. Eksp. Teor. Fix. 15, 739 (1945); 19, 36 (1949).

[3] A. F. Devonshire, Adv. Phys. 3, 85 (1954).

[4] T. R. Koehler and N. S. gillis, Phys. Rev. B 7, 4980 (1973); 13, 4183 (1976).

[5] M. E. Lines and A. M. Glass, *Principles and Applications of Ferroelectrics and Related Materials*, (Clarendon, Oxford, 1979).

[6] R. P. Feynman and H. Kleinert, Phys. Rev. A 34, 5080 (1986).

[7] R. Giachetti and V. Tognetti, Phys. Rev. B 33, 7647 (1986).

[8] A. S. Chaves, F. C. S. Barreto, and L. A. A. Ribeiro, Phys. Rev. Lett. 37, 618 (1976).

[9] H. Vogt, Phys. Rev. B 51, 8046 (1995).

[10] M. Takesada, T. Yagi, M. Itoh and S. Koshihara, J. Phys. Soc. Jpn. **72**, 37 (2003).

[11] T. Hasegawa, S. Mouri, Y. Yamada and K. Tanaka, J. Phys. Soc. Jpn. **72**, 41 (2003).

[12] H. Katsu, H. Tanaka and T. Kawai, Jpn. J. Appl. Phys. **39**, 2657 (2000).

[13] H. A. Lorentz, *The Theory of Electrons*, (Dover, New York, 1952).

[14] W. Cochra, Phys. Rev. Lett. 3, 412 (1959); Adv. Phys. 19, 387 (1960); 20,401 (1961).

[15] P. W. Anderson, *In Fizika Dielectrikov* (ed. G. I. Skanavi). Akad. Nauk. SSSR, Moscow (1960).

[16] A. S. Barker and M. Tinkham, Phys. Rev. 125, 1527 (1962).

[17] R. A. Cowley, Phys. Rev. Lett. 9, 159 (1962); Phys. Rev. 134, A981 (1964); Adv. Phys. 12, 421 (1963).

[18] E. samuelsen, E. Anderson, and J. Feder, eds., *Structural Phase Transitions and Soft Modes*, (Universitetsforlaget, Oslo, 1971).

[19] J. F. Scott, Rev. Mod. Phys. 46, 83 (1974).

[20] R. Blinc and B. Zeks, Soft Modes in Ferroelectrics and Antiferroelectrics, (Am. Elsevier, New York, 1974).

[21] T. Sakudo and H. Unoki, Phys. Rev. Lett. 26, 851 (1971).

[22] H. Uwe and T. Sakudo, Phys. Rev. B 15, 337 (1977); 13, 271 (1976); J. Phys. Soc. Jpn. **38**, 183 (1975).

[23] H. Uwe, H. Unoki, Y. Fujii, and T. Sakudo, Solid State Commun. 13, 737 (1973).

[24] G. A. Samara and B. Morosin, Phys. Rev. B 8, 1256 (1973).

[25] P. A. Fleury and J. M. Worlock, Phys. Rev. 174, 613 (1968).

[26] G. Shirane and Y. Yamada, Phys. Rev. 177, 858 (1969).

[27] R. C. Miller and W. G. Spitzer, Phys. Rev. 129, 94 (1963).

[28] A. S. Barker, Jr. and J. J. Hopfield, Phys. Rev. 135, A1732 (1964).

[29] Y. Fujii and T. Sakudo, J. Phys. Soc. Jpn. **41**, 888 (1976).

[30] B. D. Silverman and R. I. Joseph. Phys. Rev. 129, 2062 (1963).

[31] R. P. Lowdnes, Phys. Rev. Lett. 27, 1134 (1971); J. Phys. C 4, 3083 (1971).

[32] G. A. Samara and P. S. Peercy, Phys. Rev. B, 7, 1131 (1973).

[33] A. S. Barker, Phys. Rev. 136, A1290 (1964).

[34] H. Frölich, *Theory of Dielectrics*, (Clarendon, Oxford, 1949).

[35] E. M. Brody and H. Z. Cummins, Phys. Rev. Lett. 21, 1263 (1968); 23, 1039 (1969).

[36] C. H. Rerry and T. F. McNelly, Phys. Rev. 154, 456 (1967).

[37] V. Dvorák, Phys. Rev. 167, 525 (1968).

[38] P. A. Fleury and P. D. Lazay, Phys. Rev. Lett. 26, 1331 (1971).

[39] R. P. Lowndes, Phys. Rev. Lett. 27, 1134 (1971); Phys. Rev. B 6, 1490 (1972); 6, 4667 (1972).

[40] W. G. Spitzer, R. C. Miller, D. A. Kleinman, and L. E. Howarth, Phys. Rev. **126**, 1710 (1960).

[41] L. Mattheiss, Phys. Rev. B **6**, 4718 (1972).

[42] T. Hasegawa, M. Shirai, K. Tanaka, J. Lumin. **87**, 1217 (2000).

[43] J. H. Barrett, Phys. Rev. 86, 118 (1951).

[44] R. Opperman and H. Thomas, Z. Phys. B 22, 387 (1975).

[45] T. Schneider. H. Beck and E. Stoll, Phys. Rev. B 13, 1123 (1976); 12, 5198 (1975).

[46] R. Morf, T. Schneider and E. Stoll, Phys. Rev. B 16, 462 (1977).

[47] D. Schmeltzer, Phys. Rev. B 28, 459 (1983); 29, 2815 (1984).

[48] E. K. h. Salje, W. Wruck, and H. Thomas, Z. Phys. B 82, 399 (1991).

[49] E. K. H. Salje, *AIP Conference Proceedings* 359, 297 (2000).

[50] K. A. Müller and H. Burkard, Phys. Rev. B 19, 3593 (1979).

[51] U. T. Höchli and L. A. Boatner, Phys. Rev. B 20, 266 (1979).

[52] D. Rytz, U. T. Höchli and H. Blitz, Phys. Rev. B 22, 359 (1980).

[53] U. T. Höchli, *Ferroelectrics* 35, 17 (1981).

[54] G. A. Samara, Physica B 150, 179 (1988).

[55] W. Kleeman, J. Dec. and B. Westwanski, Phys. Rev. B 58, 8985 (1998).

[56] W. Kleeman, J. Dec, Y. G. Wang, p. Lehnen, and S. A. Prosandeev, J. Phys. Chem. Solids 61, 167 (2000).

[57] K. Nasu, *Photo-induced Phase Transition*, (World Scientific, Singapore, 2004), and references wherein.

[58] K. Nasu, P. Huai, and H. Mizouchi, J. Phys.: Condens. Matter 13, R693 (2001).

[59] K. Nasu, Rep. Prog. Phys. 67, 1607 (2004); Phys. Rev. B 67, 174111 (2003).

[60] X. Sun, R. L. Fu, K. Yonemitsu, and K. Nasu, Phys. Rev. Lett. **84**, 2830 (2000).

[61] C. Q. Wu, Y. Qiu, Z. An, and K. Nasu, Phys. Rev. B **68**, 125416 (2003).

[62] Z. An, C. Q. Wu, and X. Sun, Phys. Rev. Lett. **93**, 216407 (2004).

[63] M. Cappzi and A. Flova, Phys. Rev. Lett. 25, 1298 (1970).

[64] H. Unoki and T. Sakudo, J. Phys. Soc. Jpn. 23, 546 (1967).

[65] K. Nasu, *Report on 1st Naregi international nanoscience conference,* (June 14-17, 2005, Nara, Japan).

[66] T. Sekine, K. Uchinokura and E. Matsuura, Solid State Commun. **18**, 569 (1976).

[67] H. Fröhlich, Proc. Roy. Soc. A, 215, 291 (1952).

[68] T. Holstein, Ann. Phy. 8, 325 (1959).

[69] K. Nasu, Y. Toyozawa, J. Phys. Soc. Jpn. **50**, 235 (1981).

[70] A. J. Heeger, S. Kivelson, J. R. Schrieffer, and W. P. Su, Rev. Mod. Phys. **60**, 781 (1988).

[71] Y. Ono and A. Terai, J. Phys. Soc. Jpn. **59**, 2893 (1990).

[72] X. D. Wang, K. Chen and X. Sun, Syn. Met. **119**, 221 (2001).

[73] W. H. Louisell, *Quantum Statistical Properties of Radiation*, (John Wiley & Sons, New York/London/Sydney/Toronto, 1973).

[74] Y. Qiu, C. Q. Wu and K. Nasu, Phys. Rev. B **72**, 224105 (2005).